

# MAGNETOM Flash

The Magazine of MR

Supplement to Issue Number 3/2010

RSNA Edition

Not for distribution in the US.

**SIEMENS**

## Research

### Multiparametric Imaging of Tumors

*Anwar Padhani*

Page 2

### MR-PET

#### Hybrid Imaging for the Next Decade

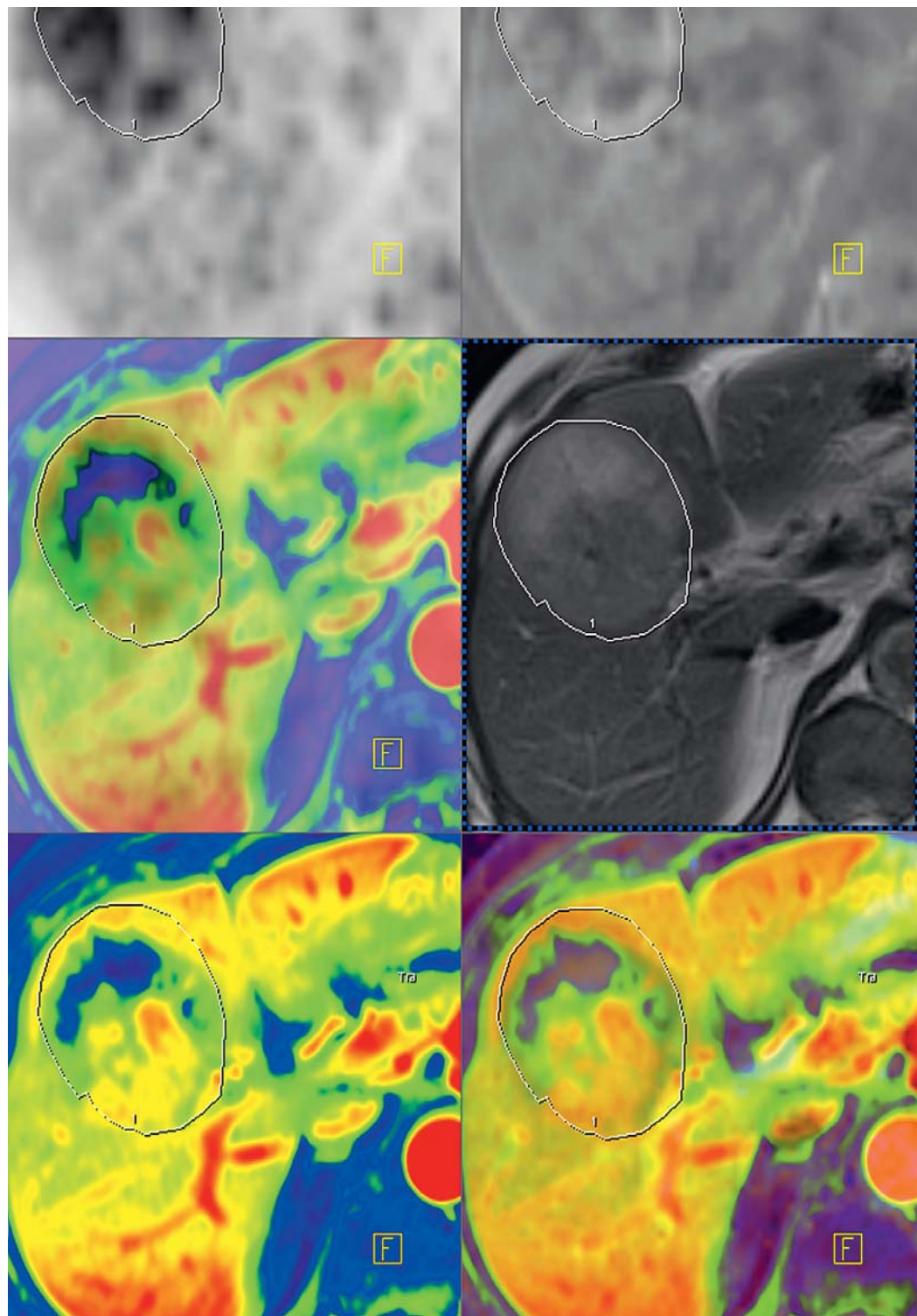
*Thomas Beyer et al.*

Page 19

### T1-weighted DCE Imaging Concepts: Modelling, Acquisition and Analysis

*Paul Tofts*

Page 30



# Multiparametric Imaging of Tumors – an Emerging Paradigm

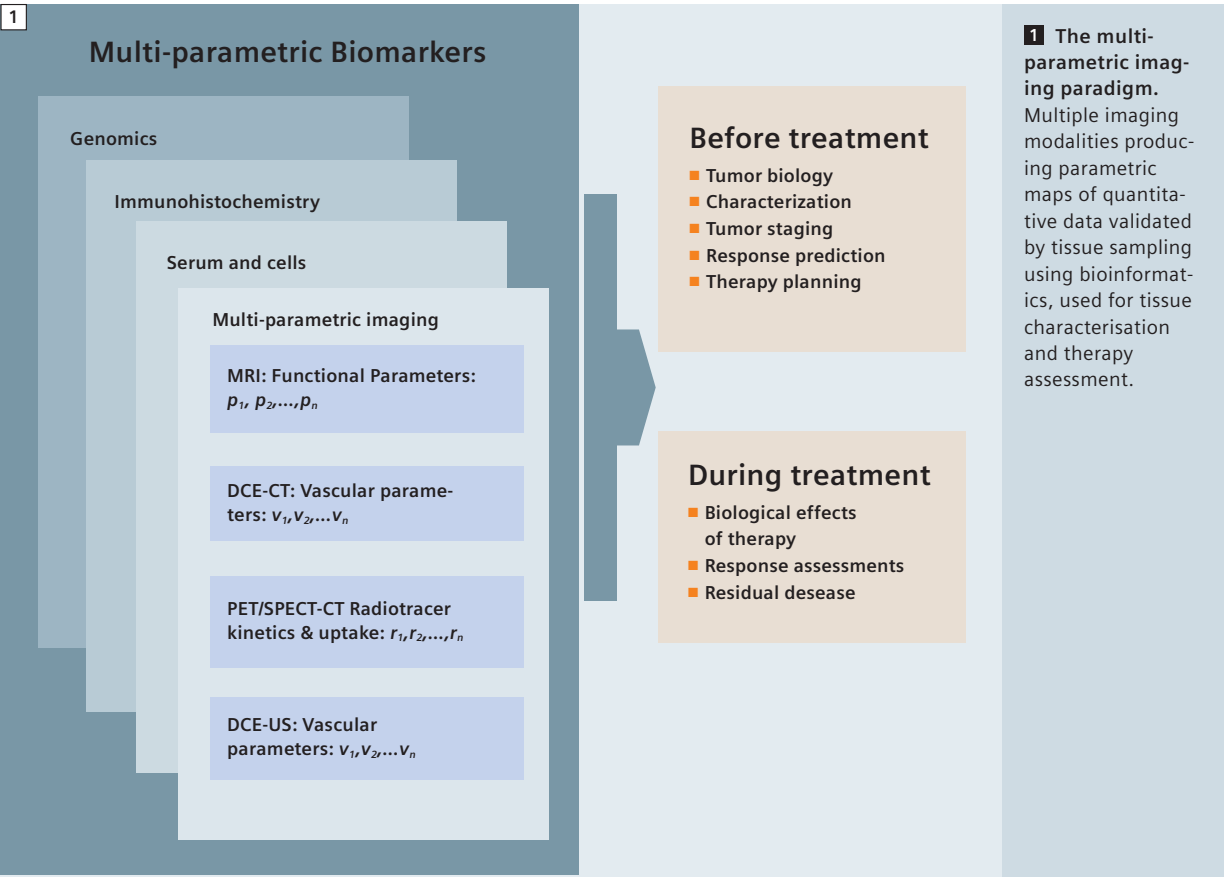
Dr. Anwar Padhani MB BS, FRCP, FRCR

Paul Strickland Scanner Centre, Mount Vernon Cancer Centre, Northwood, Middlesex, UK

## Introduction

To date, the main focus for innovations in imaging has been the achievement of excellence in anatomical resolution. In the field of cancer therapy response, morphological imaging is recognized to have significant limitations including the presence of tumors that cannot be measured, poor measurement reproducibility and mass lesions of unknown activity that persist following therapy. In neuro-oncology for example, the full extent of gliomas is poor depicted on contrast enhanced T1-images and by T2-FLAIR hyperintensity. Anatomic imaging techniques may be insensitive to changes that inform on overall therapeutic success of cytostatic therapies, because the basic assumption that changes in tumor size reflect biological activity is violated. An example is pseudoresponse of glioblastomas treated with antiangiogenic therapy, where decreasing enhancement due to vascular normalization can be seen but with increasing mass effect and/or increasing tumor infiltration. The disconnection between anatomically determined progression free survival (PFS) and therapeutic efficacy (overall survival – OS) is recognized for a number of cytostatic therapies. The latter has recently resulted in a recommendation to withdraw the license to use the antiangiogenic drug bevacizumab for metastatic breast cancer by a committee of the US Food and Drug Administration (FDA), because improved PFS which was used for initial licensing did not ultimately result in improved OS. More sophisticated measurement methods such as tumor volume and CT density changes maybe unable to completely address these limitations. Functional-molecular imaging methods made possible by the availability of MRI and PET scanners in particular have enabled many current clinical limitations to be addressed, as well as extending the applications of imaging in medicine. Thus, over the last decade we have seen the increasing use of functional-molecular imaging in the staging of patients with cancer and for

monitoring their therapeutic response. Some of these functional-molecular imaging techniques are able to predict the success of therapy before conventional measurements of size are changed. Functional-molecular parameters are also being used as pharmacodynamic biomarkers in early phases of drug development (preclinical and clinical), in order to provide confidence to proceed to more expensive clinically studies of therapeutics with novel mechanisms of action. Advantages of functional-molecular imaging techniques include the fact that quantitative biomarkers obtained are spatially resolved, although resolution is in general less than corresponding anatomical images. Moreover functional-molecular imaging techniques are now beginning to identify the emergence of therapy resistance to a variety of treatments including novel drugs. An example of the latter is new internal enhancement on CT/MRI scans or <sup>18</sup>FDG-PET uptake in a size stable gastrointestinal tumor (GIST) treated with imatinib mesylate. Examples of clinically deployed functional imaging MRI and PET techniques and the biological properties that they depict are given in tables 1 & 2. Reviews of the physical basis for MRI and PET and their differing sensitivity to depict biological processes, reveals that MRI is more suited to evaluating the structure and dynamic aspects of microenvironment of tissues (e.g., blood flow, vascular permeability, cell packing, necrosis and pH), some of which requires the administration of exogenous contrast agents or other methods of enhancing MRI sensitivity (e.g., by hyperpolarisation). On the other hand, because PET has a great sensitivity to compounds present at nanomolar or even picomolar concentrations but has a slower mode of acquisition, it is more suited to evaluating cellular and molecular processes (depending largely on the radiotracers used). Until recently, these techniques were used mostly in isolation. However, there is now an increasing possibility to undertake multifunctional/multiplex imaging



(Kobayashi, Longmire et al. 2010) for biological investigations in animals but also clinically (Antoch and Bockisch 2009; Padhani and Miles 2010). Combined/multiplex approaches have been made possible by (a) the development of hybrid imaging technologies such as SPECT-CT and PET-CT and the soon to be available PET-MRI, (b) technological advancements within individual imaging modalities which enable multi-functional data acquisitions within short periods of time including the use of multiple PET isotopes with very short half lives, (c) advances in software enabling both fusion of imaging data between different imaging modalities and derivation of quantitative biologically relevant biomarker data that can be co-registered with anatomical images, and lastly (d) bioinformatics allowing integration of quantitative imaging parameters with other biological data such as serum cytokines, circulating cells and tissue genomic and protein expressions levels from targeted tissue biopsies (Figure 1). We have come to recognize that the multiparametric imaging approach is fast becoming an important means for biological investigation because of its multi-

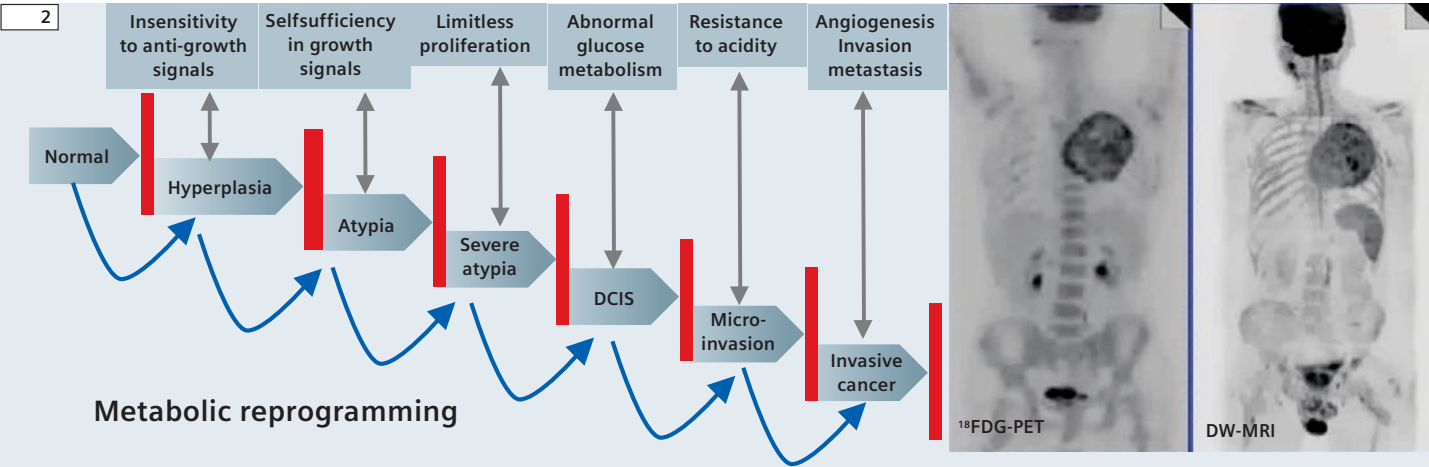
dimensional (multispectral, multispatial and temporally resolved) nature. In this article we do not discuss the technological advances that have made multiparametric imaging a reality. Instead we will appraise the current clinical roles of multiparametric imaging for characterizing tumors and in the therapy response setting indicating the added value imparted by this new approach. In so doing we can gain insights into the potential future areas where multiparametric approaches with combined PET-MRI maybe able to take us both scientifically and clinically.

**Imaging depiction of altered tumor biology**

Observations show us that cancers are complex, evolving, multiscale systems that are characterized by profound spatial and temporal heterogeneity in their biological characteristics. Most clinically manifested invasive epithelial cancers have typical, hallmark characteristics as a result of genetic changes and metabolic reprogramming that enables pre-cancer lesions to develop into virulent invasive tumors, by successfully

Table 1: Summary of commonly available functional MRI techniques, the quantitative parameters derived and their biological correlates.

Functional Imaging Technique	Biological property on which imaging is based	Commonly derived quantitative imaging parameters/ biomarkers	Pathophysiological correlates
Diffusion-weighted MRI (DW-MRI)	Diffusivity of water	<ul style="list-style-type: none"><li>Apparent diffusion coefficient (ADC)</li><li>Fractional anisotropy (FA)</li><li>Water diffusivity (D)</li><li>Perfusion fraction (<math>F_p</math>)</li></ul>	Cell density and distribution of cell sizes, extracellular space tortuosity, gland formation, cell membrane integrity, necrosis, fluid viscosity
Dynamic contrast-enhanced MRI (DCE-MRI)	Contrast medium uptake rate in tissues, which is influenced by: <ul style="list-style-type: none"><li>Perfusion &amp; transfer rates</li><li>Extra-cellular volume</li><li>Plasma volume fraction</li></ul>	<ul style="list-style-type: none"><li>Initial area under gadolinium curve (IAUGC)</li><li>Transfer and rate constants (<math>K^{trans}</math>, <math>k_{ep}</math>)</li><li>Leakage space fraction (<math>v_e</math>)</li><li>Fractional plasma volume (<math>v_p</math>)</li></ul>	Vessel density Vascular permeability Perfusion Tissue cell fraction Plasma volume
Dynamic susceptibility contrast MRI (DSC-MRI)	Blood volume and blood flow	<ul style="list-style-type: none"><li>relative blood volume/flow (rBV/rBF)</li><li>Mean transit times (MTT)</li><li>Vessel size index</li></ul>	Vessel density Blood flow Tumor grade Vessel diameter
<sup>1</sup> H-MR spectroscopic imaging ( <sup>1</sup> H-MR-SI)	Cell membrane turnover/energetics and replacement of normal tissues	<ul style="list-style-type: none"><li>Quantified ratios of metabolites including choline, creatine, lipids, citrate, lactate and others depending on echo time and tissues evaluated</li></ul>	Tumor grade Proliferation index
Blood oxygenation level dependent (BOLD) or intrinsic susceptibility-weighted (ISW) MRI	Deoxyhaemoglobin shows higher relaxivity than oxyhaemoglobin. Measurement also reflect blood volume, perfusion and Intrinsic composition of tissues	<ul style="list-style-type: none"><li>Intrinsic tissue relaxation rate (<math>R2^* = 1/T2^*</math>)</li></ul>	Tissue susceptibility properties including air and bone interfaces, ferromagnetic properties and blood oxygenation



**2 Carcinogenesis: hallmarks and metabolic reprogramming.** In the transition from normal cells to clinically manifested invasive cancers, typically phenotypic characteristics become manifested (the hallmarks of cancers) resulting from metabolic reprogramming. Functional imaging techniques can depict these metabolic processes and cancer hallmarks at the tumor level, in peritumoral regions and at the organ/whole organism levels. The whole-body images on the right side of the image are of a patient with non-small cell lung cancer imaged with <sup>18</sup>FDG-PET and DW-MRI.

adapting or circumventing the body's natural micro-environmental barriers to uncontrolled proliferation (Figure 2). These hallmarks must be present in order to sustain tumor growth and for tumors to spread (Hanahan and Weinberg 2000). These genetic changes and metabolic reprogramming often occurs in a step-wise fashion as epithelial lesions develop from normal → hyperplasia → dysplasia → carcinoma-in-situ → local invasive cancers → metastatic cancers as described by Gatenby and Gillies (Gatenby and Gillies 2008). Imaging techniques can depict some of these molecular and functional aberrations (directly or by inference) within precancerous (e.g., polyps) and cancerous lesions, in peritumoral regions and at the organ/whole organism levels. Many key cancer hallmarks can be mapped including altered metabolism (including that of glucose, amino acids and nucleosides), tumor cell hyperproliferation and apoptosis, hypoxia, angiogenesis and aberrant neovascularity, local infiltration and distant metastases. Since there is a stepwise development of the biological aberrations in cancers so functional-molecular imaging tests maybe able to inform on

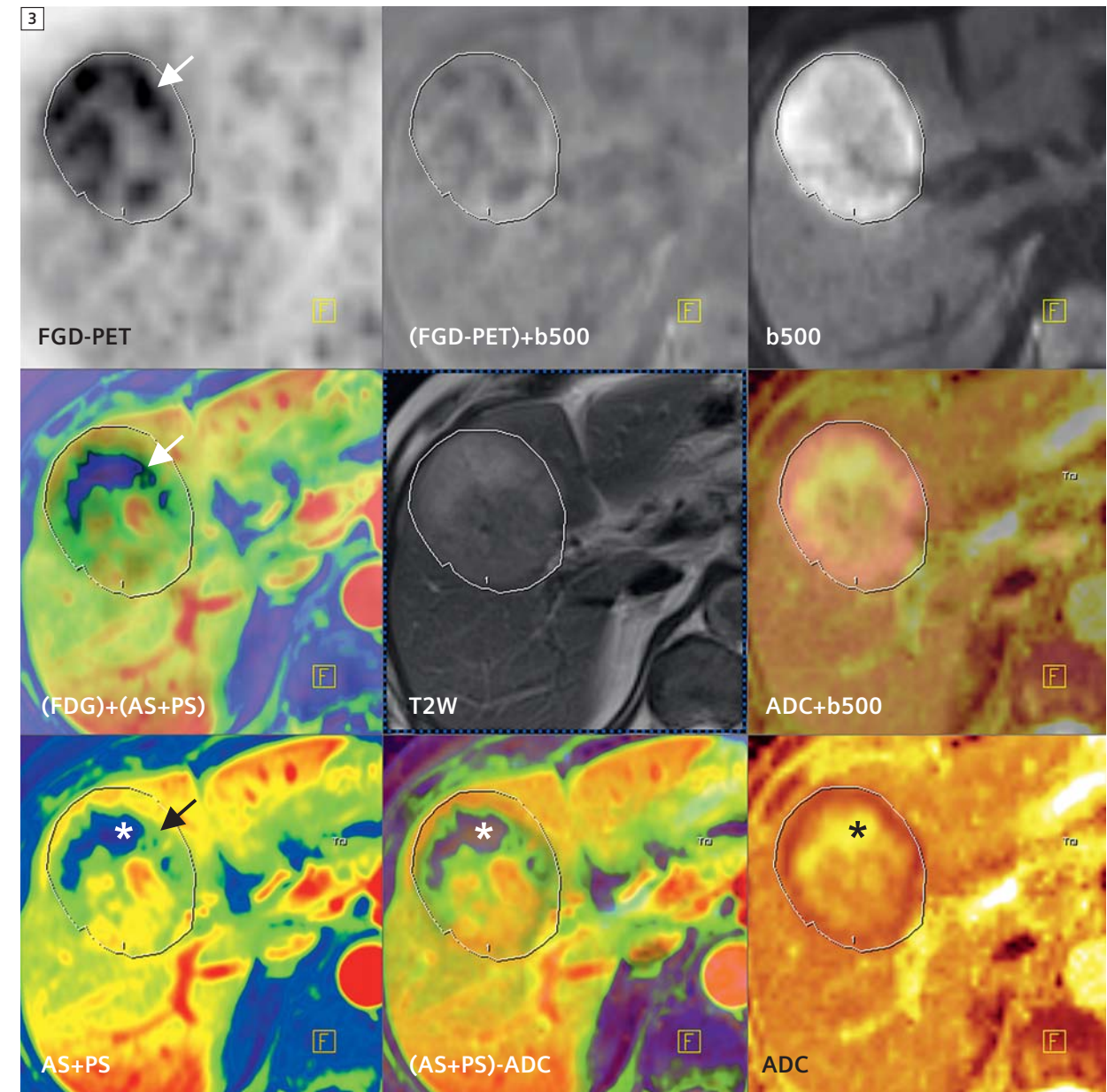
the stage of development of lesions. By combining the information derived from a number of techniques, it becomes possible to build up a unique, multi-faceted phenotypic view of tumor evolution thus allowing improved characterizations (Figure 1). As many cancer hallmarks are also key anticancer targets, the role of functional-molecular imaging can be extended into the areas of drug development and for monitoring of the clinical effectiveness of therapeutics. The rationale for the latter being that decisions regarding continuation or discontinuation of a targeted therapy could rely on specific methods that image pathways being targeted. Resistance to conventional and novel therapies is highly dependent on the tumor microenvironment and on host-tumor interactions, so the potential exists for functional-molecular imaging to inform on which patients or lesions are more or less likely to continue to respond or to develop therapy resistance. This is made possible because functional-molecular imaging depictions including the displayed heterogeneity do reflect underlying gene-protein expressions in a number of cancer types.

Continued on page 10



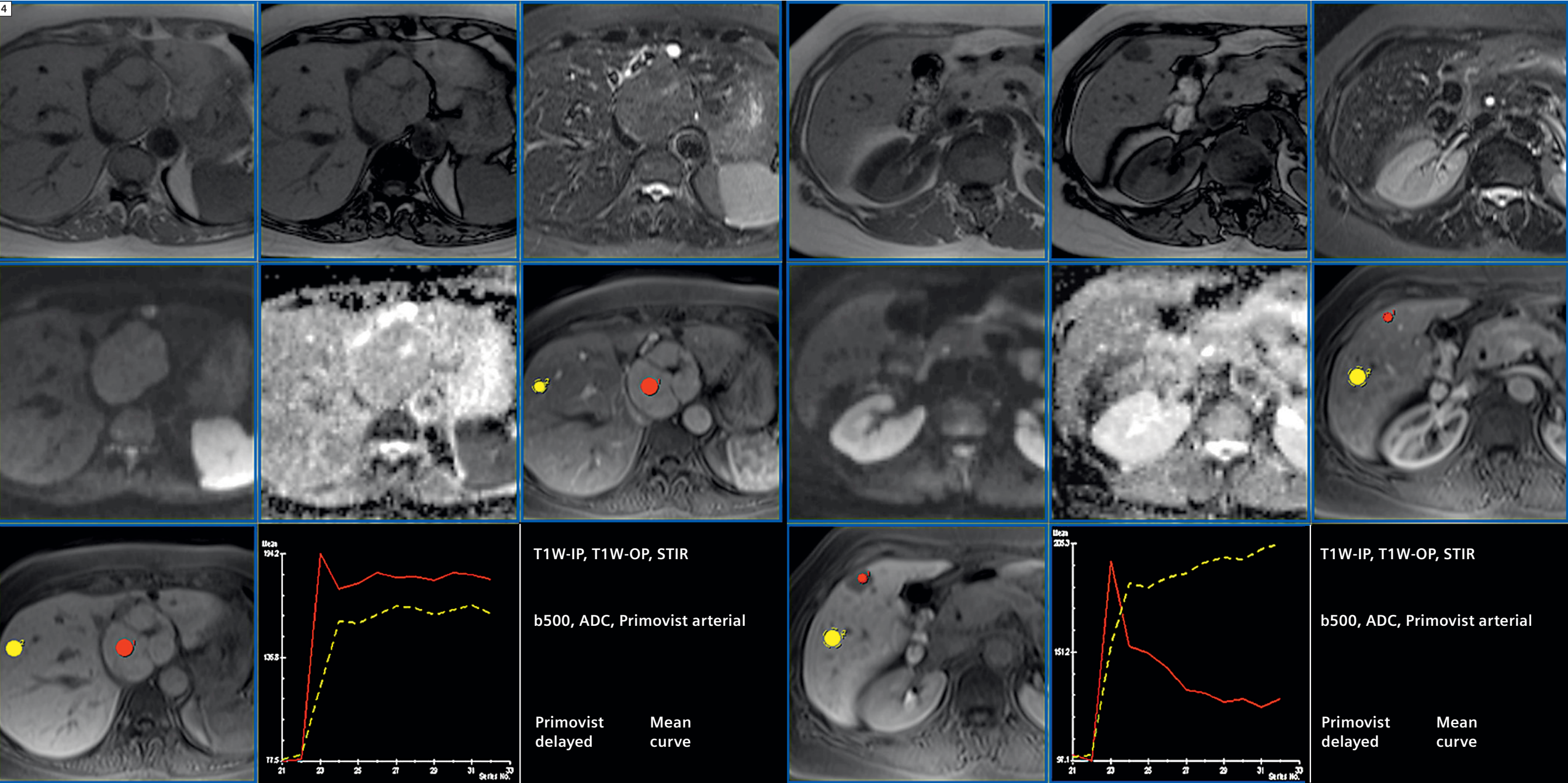
Table 2: Examples of radionuclide imaging techniques used for assessing tumors:

Radiotracer	Biological property on which imaging is based	Commonly derived quantitative imaging parameters/ biomarkers	Comments
<sup>18</sup> Fluorodeoxyglucose (FDG)	Glucose metabolism	<ul style="list-style-type: none"><li>Standardised uptake value (SUV)</li><li>Tumor to background uptake ratio</li><li>Metabolic rate of glucose</li></ul>	Up-regulation of GLUT-1 transporters and hexokinase II activity Some normal tissue have background activity – e.g., brain, liver
<sup>15</sup> O-Water	Perfusion	<ul style="list-style-type: none"><li>Perfusion (ml/(g*min))</li><li>Standardised uptake value</li><li>Tumor to background uptake ratio</li></ul>	Angiogenesis, vascularity, blood flow
<sup>18</sup> Fluorothymidine (FLT)	Cellular proliferation	<ul style="list-style-type: none"><li>Standardised uptake value</li><li>Tumor to background uptake ratio</li></ul>	Activity of cytosolic thymidine kinase Incorporation into newly synthesized DNA Does not cross blood brain barrier
<sup>124</sup> I Annexin-V	Apoptosis	<ul style="list-style-type: none"><li>Standardised uptake value</li><li>Tumor to background uptake ratio</li></ul>	Exposure of phosphatidylserine in the cell membrane during programmed cell death
<sup>99</sup> Tcm Methoxyisobutyl-isonitrile (MIBI)	pGlycoprotein mediated multi-drug resistance	<ul style="list-style-type: none"><li>Tumor to background uptake ratio</li></ul>	Ejection of cytotoxic drugs from tumor cells
<sup>18</sup> Fluoromisonidazole (MISO)	Hypoxia	<ul style="list-style-type: none"><li>Tumor to blood ratio</li></ul>	Tissue oxygenation Nitroreductase activity
Copper-diacetyl-bis (N4-methylthiosemicarbazone) (Cu-ATSM)	Hypoxia	<ul style="list-style-type: none"><li>Tumor to muscle ratio</li></ul>	Tissue oxygenation
<sup>11</sup> C-choline and <sup>18</sup> F-choline	Cellular proliferation	<ul style="list-style-type: none"><li>Standardised uptake value</li><li>Tumor to background uptake ratio</li></ul>	Cell membrane synthesis and breakdown
<sup>18</sup> F-FET and <sup>11</sup> C-methionine	Amino acid metabolism	<ul style="list-style-type: none"><li>Standardised uptake value</li></ul>	Indicates proliferative activity Useful for brain tumor recurrence



**3 Fusion imaging of MRI and FDG-PET.**  
56-year-old male with metastatic colorectal cancer to the liver. Morphological T2-weighted, DW-MRI (b500 and ADC), DCE-MRI (arterial slope (AS) and portal slope (PS) added to yield total flow) and <sup>18</sup>FDG-PET scans were combined using fusion software. Region of interest around the tumor outline on the b500 images was copied onto all images to aid cross correlations. The area of non-enhancement (\*) on the (AS+PS) image has the highest ADC values indicating necrosis. Around the area of necrosis, perfusion is decreased (green color) compared to adjacent normal liver (yellows and reds). Note that FDG uptake is greatest at the edge of necrosis in the low vascularity area (arrows) possibility related to upregulated glucose transporters (Glut-1) secondary to hypoxic stress. Higher cellular density (low ADC values) coincides with well vascular tissues where FDG uptake is relative similar to that of the liver.





Fibro Nodular Hyperplasia (FNH)

Liver adenoma

**4** **Multiparametric MRI for liver lesion characterization.**Two benign liver lesions (Fibronodular hyperplasia (FNH) and adenoma) evaluated by multifunctional MRI. Each lesion is depicted using T1w sequences (in-phase and opposed-phase), STIR sequences, DW-MRI (b500 and ADC) and DCE-MRI using a liver specific contrast agent Gadoteric acid (Eovist in the USA and Primovist outside

the USA). The different curve shapes on DCE-MRI reflect the relationship between histological structure (atretic canaliculi in FNH and no biliary canaliculi in adenomas) and functionality of contrast media transporters present on the portal and biliary sides of hepatocytes. Such structural-functional relationships can be used to more confidentially characterize liver lesions.



Continued from page 5

## Roles of multiparametric imaging

A review of the current literature shows that the multiparametric approach is used in a number of clinical areas:

### (1) For the improved depiction of biological features

Multifunctional evaluations make it possible to correlate observations between imaging biomarkers at the tumor or voxel levels. Such cross correlations can be used to:

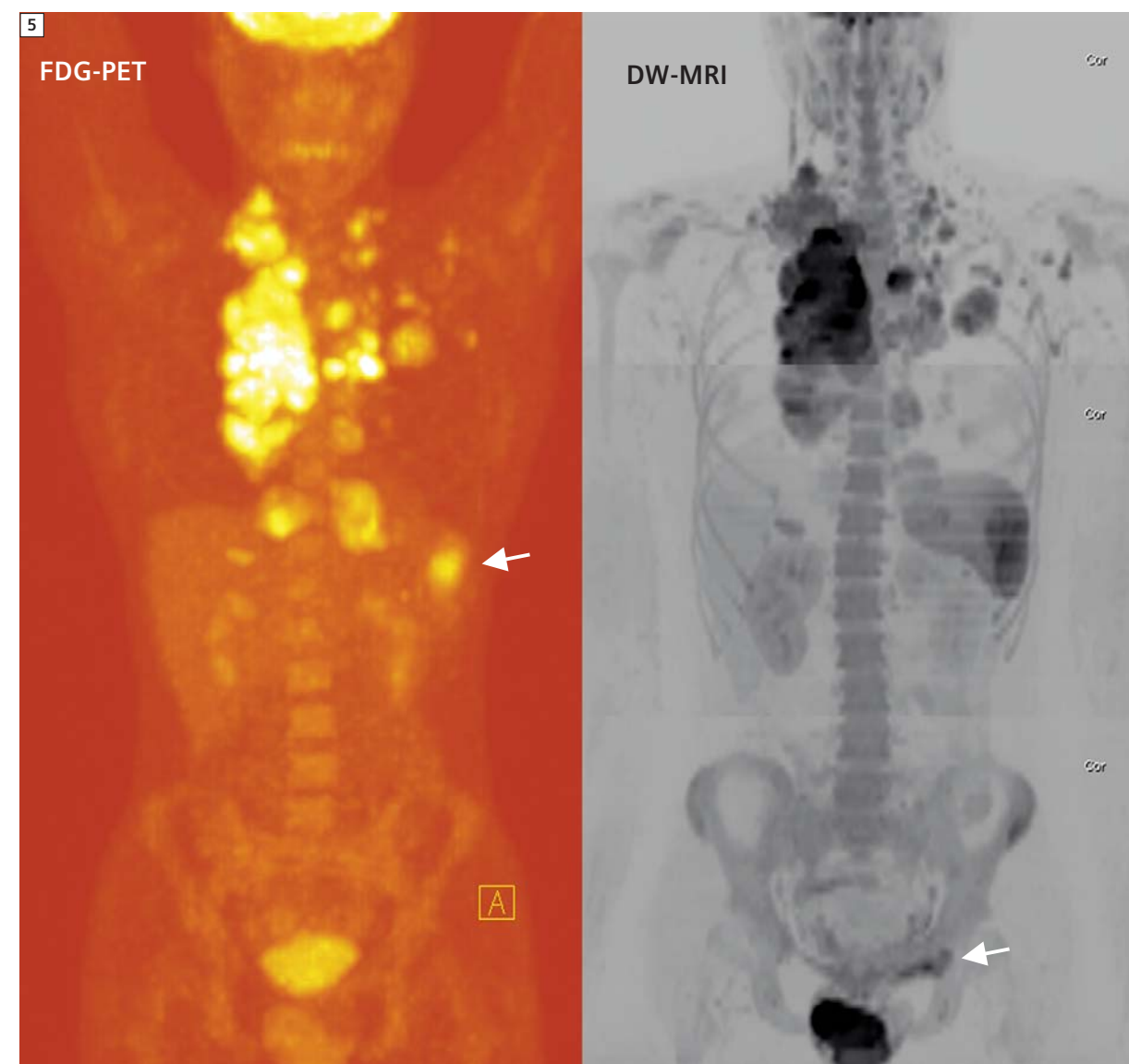
- refine the interpretation of imaging observations made by one technique using corresponding data from another. An example is the improved depiction of tissue oxygenation using BOLD-MRI by using blood volume distribution from DSC-MRI (Padhani, Krohn et al. 2007).
- To validate an emerging biomarker against an accepted standard (by ascertaining the strength of relationships between them and by exploring the circumstances under which the strength of relationships may be changed). For example, transfer constant from DCE-MRI can serve as a biomarker of tumor blood flow before therapy (because of a high first pass extraction of low molecular weight contrast agents in tumors). However, in the brain (because of an intact blood brain barrier) or when tumors are successfully treated, transfer constant becomes a biomarker of vascular permeability.
- To clarify the spatial relationships between depicted biological functions at the voxel level, so as to gain insights into the consequences of tumor metabolic reprogramming (Figure 3). For example, correlating tissue oxygenation and perfusion or perfusion and glucose metabolism has been shown to be useful for tissue characterization and for predicting therapy response as discussed below.

### (2) For clinical characterisation of known disease

Functional-molecular imaging is often used to clarify the nature of abnormalities seen on morphological tests such as a CT or ultrasound scan. Multifunctional evaluations are a natural extension of this approach which has found roles in the characterization of lesions at a variety of anatomical sites including the brain, salivary glands, liver and prostate gland. So if an indeterminate liver lesion is found using anatomic CT/US imaging, then a multifunctional MRI scan may be performed (including chemical shift imaging, diffusion MRI and dynamic contrast enhancement with a non-specific or

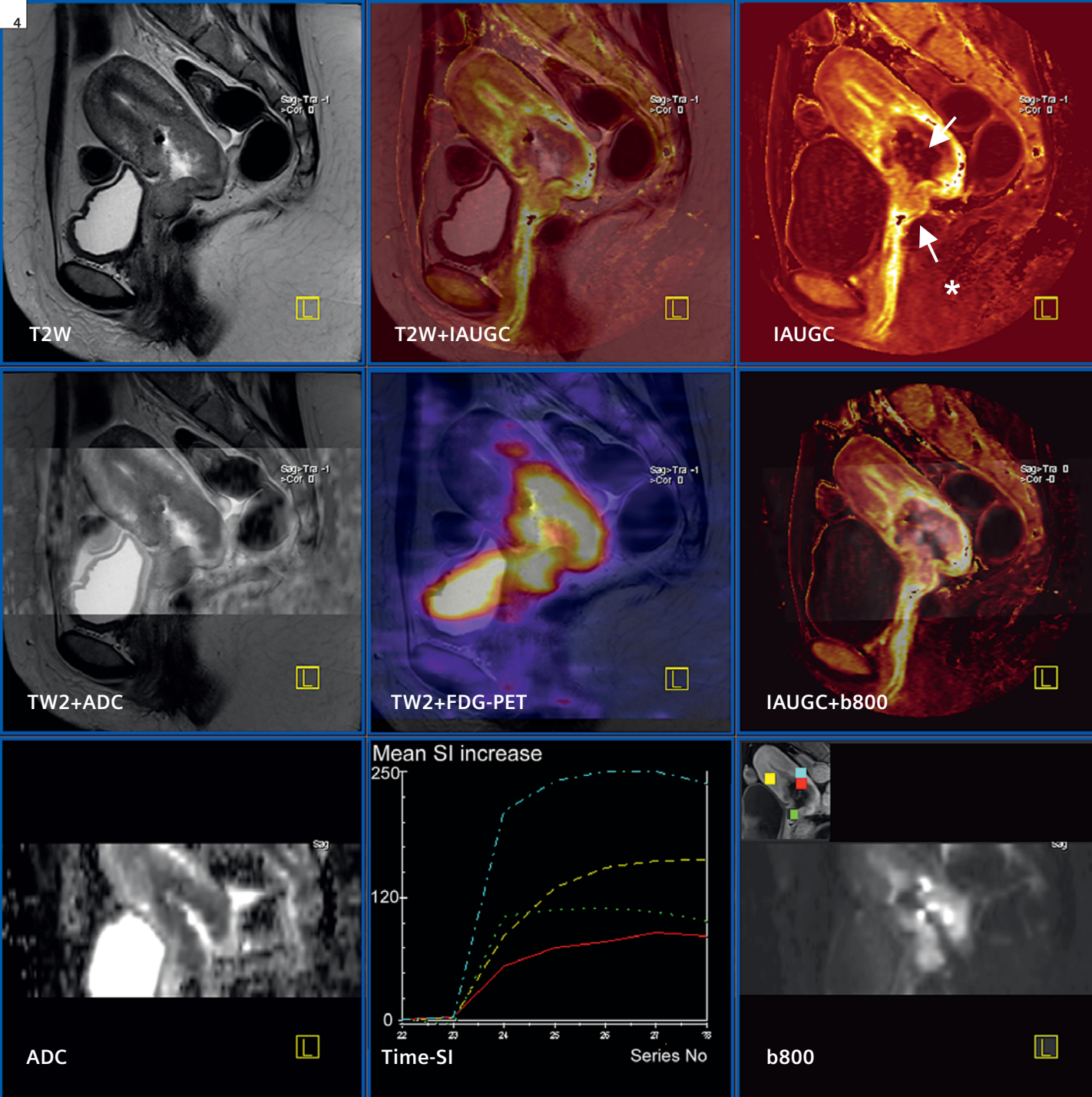
liver specific contrast agent) (Figure 4). An unhelpful MRI scan may result in the use of a further imaging test such as an  $^{18}\text{F}$ FDG-PET for further clarification. When multifunctional assessments are used for disease detection and characterisation, it may be found that individual modalities are discordant at the regional or tumor level. Discordance can occur because of tumor biology (see below) or for technical reasons including the fact that individually techniques have areas of strength and weakness, which can be overcome by combining imaging modalities together. An example is the improved staging of lymphoma by the combined use of  $^{18}\text{F}$ FDG-PET and diffusion-weighted MRI (DW-MRI).  $^{18}\text{F}$ FDG-PET is not sensitive enough for the detection of bone marrow infiltration which can be partially overcome by using DW-MRI. On the other hand DW-MRI is not sensitive enough to detect splenic disease which can be detected by  $^{18}\text{F}$ FDG-PET (Figure 5).

Discordant results can also be biologically meaningful often provoking new lines of investigations into tumor structural-functional relationships. For example, a number of studies have evaluated the relationship between glucose metabolism ( $^{18}\text{F}$ FDG-PET) and tissue perfusion (which can be done with  $^{15}\text{O}$ -water-PET, perfusion-CT and dynamic susceptibility contrast MRI (DSC-MRI)). The recently introduced capability to perform perfusion-CT/ $^{18}\text{F}$ FDG-PET has broadened the availability of this multiparametric approach. Although tightly coupled in most normal tissues, many studies have shown that the relationships between blood flow and glucose metabolism is not well matched in all tumors. Flow-metabolism mismatches have been shown in many tumor types depending on spatial location within tumors, on tumor type and grade, size and stage (Miles and Williams 2008). Miles and Williams suggested that low vascularity with high glucose uptake represents appropriate metabolic tumor adaptation to hypoxic stress whereas low vascularity with low glucose uptake represents a failure of tumor adaptation (Figures 6). Importantly the adaptive response (i.e., high glucose metabolism relative to blood flow) has been shown to be associated with poorer patient outcomes in breast and pancreatic cancers (Mankoff, Dunnwald et al. 2009). In the future, we can expect multifunctional-molecular imaging with PET-MRI systems to enable similar correlations between other biological processes to be undertaken, so as to gain greater insights into structural-functional relationships in health and disease and how these are altered in response to therapy.



**5 Improved lymphoma staging with whole-body  $^{18}\text{F}$ FDG-PET and DW-MRI.** 23-year-old male with Hodgkin's lymphoma. Nodal distribution of disease between whole-body  $^{18}\text{F}$ FDG-PET and DW-MRI is very similar. The  $^{18}\text{F}$ FDG-PET scan shows a splenic deposit (arrow on the PET scan) which is not visible on the DW-MRI (where only normal increased signal intensity is seen). On the other hand the bone marrow abnormality seen in the left superior pubic ramus on the DW-MRI (arrow) is not appreciated on the PET scan. Both lesions were unproven histologically because their presence does not affect the therapy to be given. There is some variation in the signal intensity of the top station of the DW-MRI compared to the middle and lower stations.





**6 Fusion imaging of morphology MRI with DW-MRI, DCE-MRI and  $^{18}\text{F}$ -FDG-PET** 30-year-old female with non-metastatic poorly differentiated squamous carcinoma of the cervix. T2-weighted and DCE-MRI (initial area under gadolinium curve – IAUGC) was performed in the sagittal plane. DW-MRI (b800 s/mm<sup>2</sup> and ADC maps) and  $^{18}\text{F}$ -FDG-PET scans were acquired in the axial plane and reconstructed into the sagittal plane. Top row images (left to right): T2-weighted (T2w), T2w image fused with initial area under gadolinium curve (IAUGC) and IAUGC maps. Middle row (left to right): fused T2w with ADC, T2w image fused with FDG-PET scan and IAUGC fused with b800 image. Bottom row (left to right) ADC map, time signal-intensity curves for regions of interest indicated in small insert on top of the b800 diffusion-weighted image. Note that the entire tumor depicted on T2w image is hypercellular (high signal intensity on b800 image and low on ADC map), hypermetabolic on the PET scan but the degree of vascularity is not uniformly distributed. The large hypovascular region (down arrow; red curve on the time-SI curves) has high glucose metabolism (adaptive response) which is likely to be more hypoxic than the anterior lip of the cervix (upward arrow with \*) which is more vascular (green line). It is in adaptive areas (low flow with high glucose metabolism) where more aggressive tumor cell clones have been noted to emerge.

### (3) Improved understanding of the biological effects of therapies

Monitoring changes during therapy with multifunctional imaging can provide invaluable information on the *in-vivo* mechanisms of action of therapeutics and of likely patients' outcomes. A number of studies have reported on the multiparametric approach for monitoring the effects of conventional therapies and for drugs with novel mechanisms of action. With respect to the latter, large numbers of new therapeutics are being developed as a result of the improved understanding of the molecular and genetic pathways controlling cellular function. Targeted molecular approaches typically seek to inhibit specific characteristics that are specific to cancers. As the pharmaceutical industry moves towards increasingly complex multi-targeted therapies, the anticipated effects on tumor tissues *de-novo* has become more difficult to predict. There is a growing recognition that biomarkers (including those derived from functional-molecular imaging) will play increasingly important roles in the drug development process (Figure 1). Imaging biomarkers can be used to confirm mechanisms of action of drugs *in-vivo* in early phase pre-clinical and clinical studies. Such pharmacodynamic (PD) data can then be potentially be harnessed for making "go-no-go" decisions at early stages of drug development; an important aim of which is to reduce the risk of failure of higher cost pivotal trials.

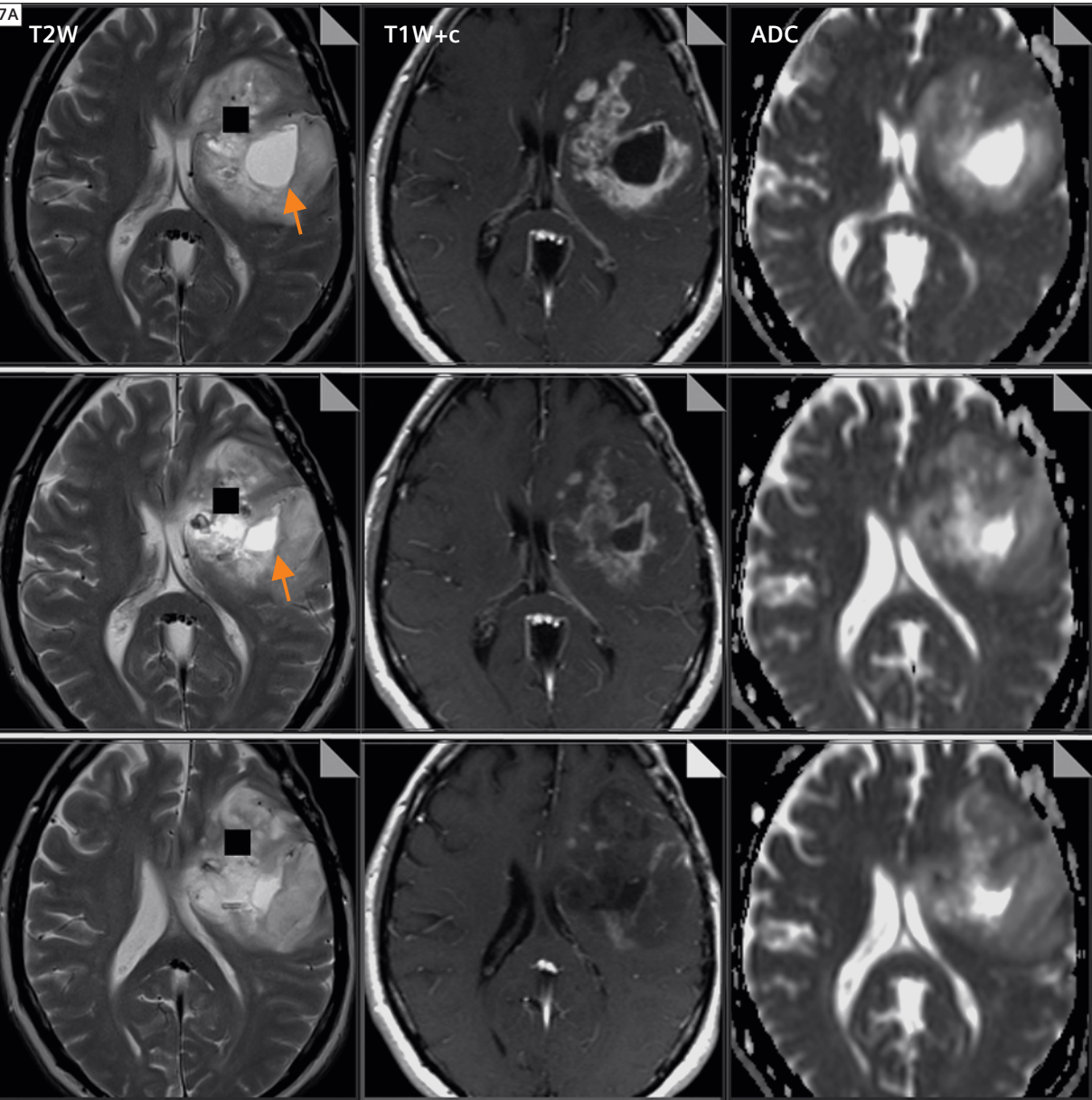
It is increasing being recognized that multiple tumor microenvironmental characteristics such as oxygenation levels, perfusion, extracellular pH, glucose metabolism and interstitial pressure as well as host-tumor interactions are important determinants of response to therapy, also determining the subsequent development of therapy resistance. For example, Batchelor et al. recently evaluated the antiangiogenic drug cediranib, given as monotherapy to patients with recurrent glioblastomas (Batchelor, Sorensen et al. 2007). Multiparametric MRI assessments showed rapid reductions in transfer constant, extracellular leakage space, and water diffusivity following treatment as the blood brain barrier became normalized. These effects were seen only in the enhancing volume of the tumor indicating that microenvironmental factors are determinants of therapy response. Interestingly, the enhancing tumor which had initially decreased in volume began to expand despite persistent decreases in microvessel permeability (pseudoresponse) suggesting that therapy resistance had developed (Figure 7). The mechanisms for the development of therapy resistance to antiangiogenics and other novel therapies are still being evaluated and will certainly include microenvironmental factors and host-

tumor interactions. The ability to image the development of adverse characteristics leading to therapy resistance might enable us to develop strategies to circumvent such tumor adaptations, for the benefit of patients.

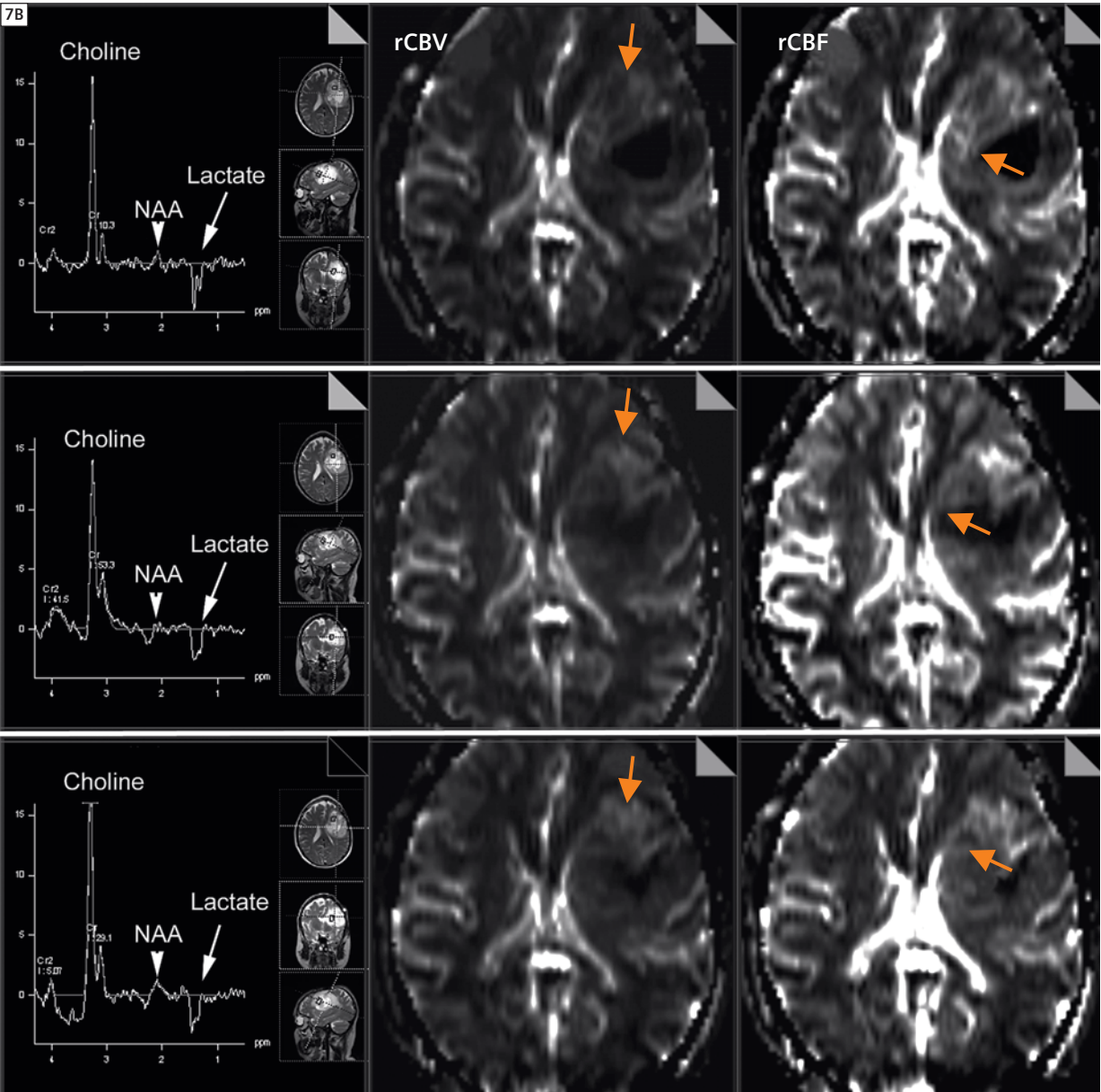
### (4) Radiation therapy planning

Advances in imaging hardware related to radiation delivery have led to improvements in the physical conformity of radiation planning, treatment and delivery to tumors and organ boundaries using conformal and intensity-modulated techniques. The additional ability to combine image-depicted biology with image-guided radiotherapy has opened the way for further refinements of target definition and dose delivery, such that it is now possible to shape-dose volume distributions not only to the geometry of targets but also to differences in the radiobiology across tumors. Imaging-depicted radiobiologically relevant characteristics include tumor grade, hypoxia, acidosis or cellular proliferation. Multiparametric imaging can potentially bring real benefits for radiation therapy planning in patients with brain gliomas where tumor delineation and gauging the aggressiveness of cancers by conventional contrast enhanced MRI/CT is severely limited (Dhermain, Hau et al. 2010). Uncoupling between tumor cell distribution and tumor grade makes it difficult to define effective, yet safe, margins for radiotherapy using conventional imaging. Uniform margins will either cover too much uninvolved brain (potentially exposing eloquent brain regions to unnecessary high radiation doses) or leave areas of tumor infiltration outside the treatment volume. This conundrum can potentially be overcome by multiparametric imaging; for example by combining  $^{11}\text{C}$ -methionine PET with morphological MRI for tumor delineation and tumor grade mapping with perfusion MRI or  $^1\text{H}$ -MR Spectroscopy (MRSI). This means that PET-MRI-planning CT scans ultimately need to be mapped onto the same frame reference for the purpose of brain radiation planning. In this regard, a combined MRI-PET scanner has obvious advantages minimizing the number of steps that use image co-registration software for data fusion and to correct geometrical distortions. Proof of concept studies, mostly retrospective, have shown that such multiparametric approaches can influence the placement of radiation treatment fields for glioma patients with the potential to improve treatment outcome (Dhermain, Hau et al. 2010), because the additional functional information is expected to increase the accuracy of target and normal tissue delineations. Validation of the efficacy of this new imaging-treatment approach will be needed, if this new paradigm is to become standard of clinical care.





**7** **Multiparametric MR imaging of anti-VEGF antibody therapy.** 40-year-old man with a high grade glioma before and during anti-VEGF antibody therapy. Rows: serial images obtained before, after 14 days and after 12 weeks of bevacizumab therapy. Figure 7A shows serial changes in morphology (T2w), contrast enhancement (T1w+c) and diffusion MRI (ADC). Figure 7B shows serial changes in MR spectroscopy (TE = 135 ms) and relative blood volume (rBV) and flow (rBF).  
**Row 1:** pre-bevacizumab. The T2w image shows a large tumor with necrotic region (arrow). The T1 post-contrast image shows areas within the tumor where the blood-brain-barrier has broken down and other areas where no enhancement is seen. The ADC map shows areas of low ADC (similar to brain) and very high ADC regions indicating necrosis. The MR spectrum taken from the region of the black box region on the T2w image, demonstrates a large choline (Cho) peak which correlates with hypercellularity, a reduced N-acetylaspartate (NAA) peak showing that neurons have been destroyed or displaced, and an inverted lactate acid (Lac) peak indicating anaerobic glycolysis.



**Row 2:** 14 days post-bevacizumab. Some reduction in the size of the mass is seen particularly of the necrotic component on the T2w image. A marked reduction in contrast enhancement indicates that capillary permeability has been reduced but the MRSI has remained unchanged indicating that there has been no cell death. Note that there has been some reduction in relative cerebral blood flow (upward pointing arrow) in a small region of the tumor.  
**Row 3:** 12 weeks post-bevacizumab. The tumor has increased in size and thickness by growing into the area of necrosis. Again there is a reduction in enhancement indicating an on-going anti-permeability effect of bevacizumab. MRSI has not changed indicating the absence of tumor cell kill confirmed by the lack of change in the tumor ADC map. Increasing relative blood volume and flow (down pointing arrow) is consistent tumor progression also.



## Challenges for implementation

Multifunctional imaging observations reinforce the underlying message of this review, that it is only by combining biomarker data from a number of imaging techniques that one may begin to truly understand how tumors interact with the host and how therapies affect tumor cells and tissue microenvironments. Such observations can also provide unique insights into the mechanism of drug action *in-vivo* and useful pharmacodynamic information. However, if functional-molecular imaging is to take up its unique position of enhancing decision-making at critical milestones in drug development, or in personalized medicine where therapy is adapted according to tumor-host phenotype or in novel radiation therapy planning, then procedural rigor and validation will be needed to establish biomarker-combinations for such roles.

It is possible to acquire spatially-matched multiparametric imaging data in potentially every patient at a given time point. Currently, integration of multidimensional imaging datasets represents a major challenge. If multiparametric data is acquired several times during a treatment, then there is an added level of complexity brought on by changing morphological features and patient repositioning. Sophisticated, user-friendly software workspaces need to be developed urgently, in order to be able to integrate/cross correlate data analysis procedures so as to follow changes in response to therapy. Computer platforms need to incorporate bioinformatics approaches, so that imaging biomarkers can be correlated with findings from immunohistochemistry, gene expression profiles, and tissue and clinical biomarker data. Ultimately, multispectral imaging analyses should be able to generate probability biomaps of important biological characteristics or to infer underlying molecular gene expression patterns. Composite biomaps incorporating functional imaging would be invaluable in lesion characterisation, therapy planning and for assessing the effects of therapies.

## Conclusions

When considering the potential opportunities for multiparametric imaging to influence patients' management, it should be remembered that the perceived advantages of such approaches are currently without a sound evidence base regarding selection of patients who would benefit from these more complex approaches, and whether improved patient outcomes will ultimately be seen. Furthermore, functional-molecular imaging techniques are at different stages of development with incomplete validation or acceptance

of standards for data acquisition and analysis. Frameworks for the validation of functional-molecular imaging to support clinical decision making are only now beginning to emerge. Additionally, there are practical challenges for incorporating both anatomical-functional-molecular into therapy paradigms including image-guided radiotherapy systems, which will need to be overcome. However, we can state with some confidence that there are extraordinary opportunities for multiparametric imaging approaches to evolve into qualified biomarkers that are useful clinically, for pharmaceutical drug development, radiation therapy planning and for predicting therapeutic efficacy. Multidisciplinary efforts will be required to bring this vision into fruition.

### References

- 1 Antoch, G. and A. Bockisch (2009). "Combined PET/MRI: a new dimension in whole-body oncology imaging?" *Eur J Nucl Med Mol Imaging* 36 Suppl 1: S113-20.
- 2 Batchelor, T. T., A. G. Sorensen, et al. (2007). "AZD2171, a pan-VEGF receptor tyrosine kinase inhibitor, normalizes tumor vasculature and alleviates edema in glioblastoma patients." *Cancer Cell* 11(1): 83-95.
- 3 Dhermain, F. G., P. Hau, et al. (2010). "Advanced MRI and PET imaging for assessment of treatment response in patients with gliomas." *Lancet Neurol* 9(9): 906-920.
- 4 Gatenby, R. A. and R. J. Gillies (2008). "A microenvironmental model of carcinogenesis." *Nat Rev Cancer* 8(1): 56-61. Hanahan, D. and R. A. Weinberg (2000). "The hallmarks of cancer." *Cell* 100(1): 57-70.
- 5 Kobayashi, H., M. R. Longmire, et al. (2010). "Multiplexed imaging in cancer diagnosis: applications and future advances." *Lancet Oncol* 11(6): 589-95.
- 6 Mankoff, D. A., L. K. Dunnwald, et al. (2009). "Blood flow-metabolism mismatch: good for the tumor, bad for the patient." *Clin Cancer Res* 15(17): 5294-6.
- 7 Miles, K. A. and R. E. Williams (2008). "Warburg revisited: imaging tumour blood flow and metabolism." *Cancer Imaging* 8: 81-6.
- 8 Padhani, A. R., K. A. Krohn, et al. (2007). "Imaging oxygenation of human tumours." *Eur Radiol* 17(4): 861-72.
- 9 Padhani, A. R. and K. A. Miles (2010). "Multiparametric imaging of tumor response to therapy." *Radiology* 256(2): 348-64.

### Contact

Dr Anwar Padhani MB BS, FRCP, FRCR  
Consultant Radiologist and Head of Imaging Research  
Paul Strickland Scanner Centre  
Mount Vernon Cancer Centre  
Rickmansworth Road  
Northwood, Middlesex  
HA6 2RN  
United Kingdom  
Tel: ++44-(0) 1923-844751  
Fax: ++44-(0) 1923-844600  
anwar.padhani@stricklandscanner.org.uk

# Benefit from the outstanding presentations that we have captured during the 7. MAGNETOM World Summit

Anwar R. Padhani  
Paul Strickland Scanner Centre, Northwood, UK

Why and when to use DWI outside the brain  
and  
Prostate imaging – state-of-the-art imaging techniques



Paul Tofts  
Brighton and Sussex Medical School, Brighton, UK

Pharmakokinetic modelling – what's behind it?  
and  
Acquisition and evaluation of dynamic  
contrast-enhanced MR data



A. Gregory Sorensen  
Massachusetts General Hospital, Boston, MA, USA

Molecular imaging – basics, concepts  
and relevance for MRI



Bernd Pichler  
Laboratory for Preclinical Imaging and  
Imaging Technology, Tübingen, Germany

MR-PET technology

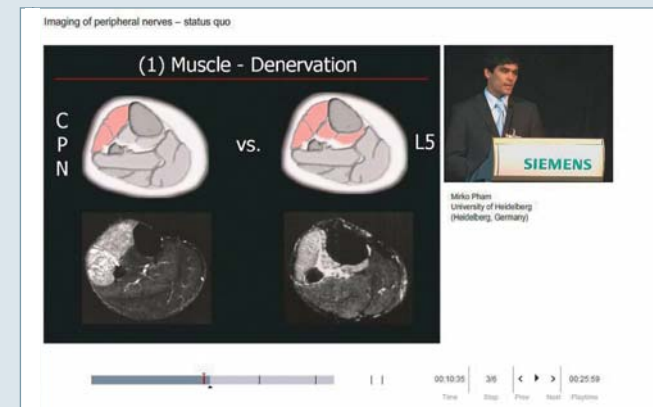


Visit us at  
[www.siemens.com/magnetom-world](http://www.siemens.com/magnetom-world)

Go to  
[International Version > e-trainings & Presentations](#)

# Relevant clinical information at your fingertips

From technology to clinical applications, you will find all the latest news on Siemens MR at [www.siemens.com/magnetom-world](http://www.siemens.com/magnetom-world)

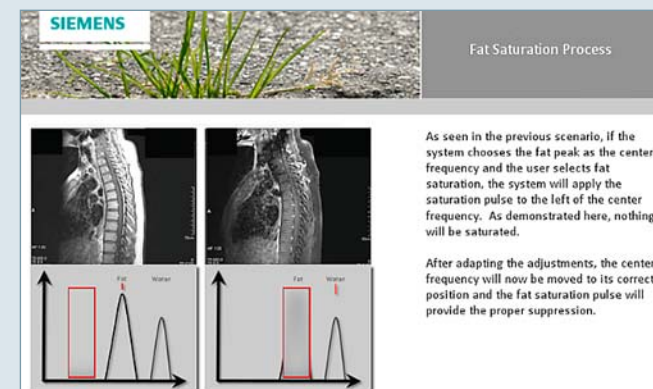


Don't miss the talks of international experts on Magnetic Resonance Imaging.

**Go to Education**  
**> e-trainings & Presentations**

The centerpiece of the MAGNETOM World Internet platform consists of our users' clinical results. Here you will find case reports and clinical methods.

**Go to Clinical Corner > Case Studies**



Just a mouse click away you will find application videos and useful tips allowing you to optimize your daily MR examinations.

**Go to Clinical Corner > Application Tips**

For the whole range of clinical MR information visit us at

[www.siemens.com/magnetom-world](http://www.siemens.com/magnetom-world)

# MR/PET – Hybrid Imaging for the Next Decade

Thomas Beyer, Ph.D.<sup>1</sup>; Nina Schwenzer, M.D.<sup>2</sup>; Sotirios Bisdas, M.D.<sup>2</sup>; Claus D. Claussen, M.D.<sup>2</sup>; Bernd J. Pichler, Ph.D.<sup>3</sup>

<sup>1</sup>Imaging Science Institute (ISI) Tübingen, University Hospital Tübingen, Germany

<sup>2</sup>Department of Diagnostic and Interventional Radiology, University Hospital Tübingen, Germany

<sup>3</sup>Laboratory for Preclinical Imaging and Imaging Technology, University Hospital Tübingen, Germany

## Dual-modality imaging

Traditionally, medical imaging is dominated by anatomical imaging, such as X-ray, ultrasound (US), computed tomography (CT) and magnetic resonance imaging (MRI). Functional imaging plays a minor, albeit important role. Most functional imaging modalities, including positron emission tomography (PET), are operated in the realms of nuclear medicine, sometimes mockingly referred to as 'unclear' medicine, so as to point to the fact that nuclear medicine images are comparatively noisy and of lower spatial resolution than, for example, CT or MR images. Nonetheless, PET in particular has been demonstrated to be of particular value in a number of disease staging and follow-up regimens. Despite the clinical usefulness of standalone nuclear medicine and radiology imaging, the desire to combine anatomical, functional (e.g. perfusion) and especially metabolic imaging has been pursued since the 1960's when physicians manually added body contours to planar scintigraphy images of the thyroid. Subsequent approaches to image fusion included side-by-side viewing of complementary image sets on film and on light boxes; image fusion was performed in the head of the physicians and mainly dominated by the personal experience and expertise. The first reliable approaches to computer-assisted image co-registration and fusion were presented in the mid 1980's in an attempt to align brain studies from MR and PET. While retrospective image alignment and fusion works usually well for the brain, similar approaches do not work as well for extra-cerebral studies that are affected by multiple degrees of patient motion. The introduction of combined, dual-modality imaging systems in the late 1990's offered for the first time the acquisition of high quality anatomical and functional / metabolic image information within a single examination. This was a unique stimulus for non-invasive diag-

nosis, and has resulted in an extraordinary rapid growth and commercial adoption of imaging systems such as SPECT (single photon emission tomography)/CT and PET/CT. A decade after its prototype introduction, PET/CT, for example, has become the modality-of-choice for a variety of clinical indications in oncology. Today, over 5,000 PET/CT systems are installed worldwide and up to 90% of all PET-investigations are performed for oncology indications with <sup>18</sup>F-FDG (fluorodesoxyglucose) being the tracer-of-choice in most of these indications. As discussed in this article, an alternative combination of MR with PET, while technically challenging, has a number of advantages compared to existing dual-modality imaging systems. Prototype MR/PET systems were first proposed for small animal imaging in the 1990's. Recently first prototype MR/PET systems were proposed for imaging humans and case reports and initial pilot studies have promoted a rising interest in this combination of two well-established diagnostic modalities.

## MR/PET: From a PET attached to a CT to a PET inside an MR

### Tracer principle

The origins of positron emission tomography date back more than 30 years. PET is a functional / metabolic imaging technique based on the detection of coincident photons originating from the annihilation of emitted positrons with electrons from surrounding tissues. PET employs biomolecules that are labeled with neutron-deficient nuclei, i.e. positron emitters. As such, the whole-body distribution of positron-emitting biomarkers can be followed and imaged with high sensitivity using PET (Fig. 1).

Upon decay of a neutron-deficient radioisotope (e.g. <sup>18</sup>F) attached to the biomolecule being traced (e.g. glucose) a positron is emitted. After traveling a mean path of



less than a mm in tissue the positron annihilates with an electron, thus creating two 511 keV photons that are emitted in opposite direction. PET scintillation detectors arranged around the patient register the annihilation photons in coincidence and store the events in sinograms from which PET activity distributions are reconstructed following the emission acquisition.

PET detector

PET detector arrangements are based on Anger readout (Fig. 2) which is in turn on light sharing and mapping many small scintillation crystals to few light detectors (in clinical PET/CT scanners usually photomultiplier tubes (PMT)). The annihilation photon (Fig. 1) is stopped in the scintillator (Fig. 2) and the energy is transformed into secondary scintillation light pulses, which produce photoelectrons at the first cathode level of the PMT, next to the entrance window. These photoelectrons are directed and amplified (multiplied) by an electric field applied to the PMT. For each annihilation photon stopped an electric pulse is generated from the scintillator-PMT detector and stored with respect to the location of the crystal depending on the Anger localization. In the 1990's, bismuth germanate (BGO) was the crystal material of choice for almost all PET systems. Today, BGO is replaced mainly by lutetium oxyorthosilicate (LSO), or variations thereof; a scintillator material that combines fast timing properties with high light output and good stopping power for 511 keV photons. Modern PET system designs include several detector rings that fully surround the patient providing an axial field-of-view (FOV) of 15–22 cm with a measured transverse FOV of up to 70 cm. Most whole-body PET systems yield an intrinsic spatial resolution of 4–6 mm. Sensitivity and spatial resolution are key parameters for PET systems and both depend directly on the properties of the scintillation crystals as part of the PET detector system.

PET/CT systems

Today, close to 70% of all installed PET units are combined PET/CT devices. All but 2 of 8 PET system vendors, who offer standalone PET systems designed for dedicated clinical tasks, offer PET systems for clinical use that are combined with a CT system. The main advantages of combined PET/CT are the intrinsic availability of co-registered functional and anatomical information from PET and CT, for local and whole-body examinations respectively alike. Second, the ability to use available CT transmission images to replace lengthy PET transmission images using 511 keV rod sources, thus reducing overall examination time significantly and limiting noise propagation from measured attenuation correction.

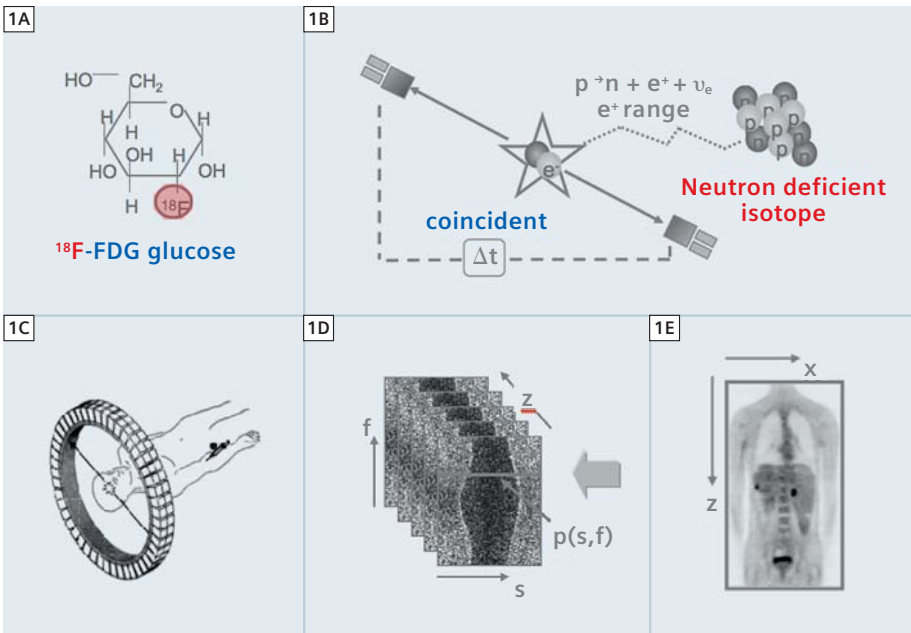
Dual-modality PET/CT systems combine a whole-body PET and a standard multi-slice CT within a single gantry. Various design concepts exist (Fig. 3), all aiming at reducing footprint and bringing the PET and CT components closer together. No fully-integrated, single-detector PET/CT exists today, however, because of the challenges to manufacture a detector system that is capable of CT (40–140 keV) and PET (511 keV) imaging. By using novel patient handling systems, patients are positioned accurately and reproducibly for co-axial imaging. Reports on residual displacements between CT and PET along the co-axial imaging range in combined PET CT indicate a maximum displacement of error of 0.5 mm. Thus, PET/CT yields the best possible alignment of extensive, complementary image volumes. With the benefits of intrinsically aligned PET and CT data, shorter overall scan times and the logistical advantages for patients and staff, combined PET/CT imaging has become a modality-of-choice for patient management in clinical oncology.

Challenges and drawbacks of PET/CT

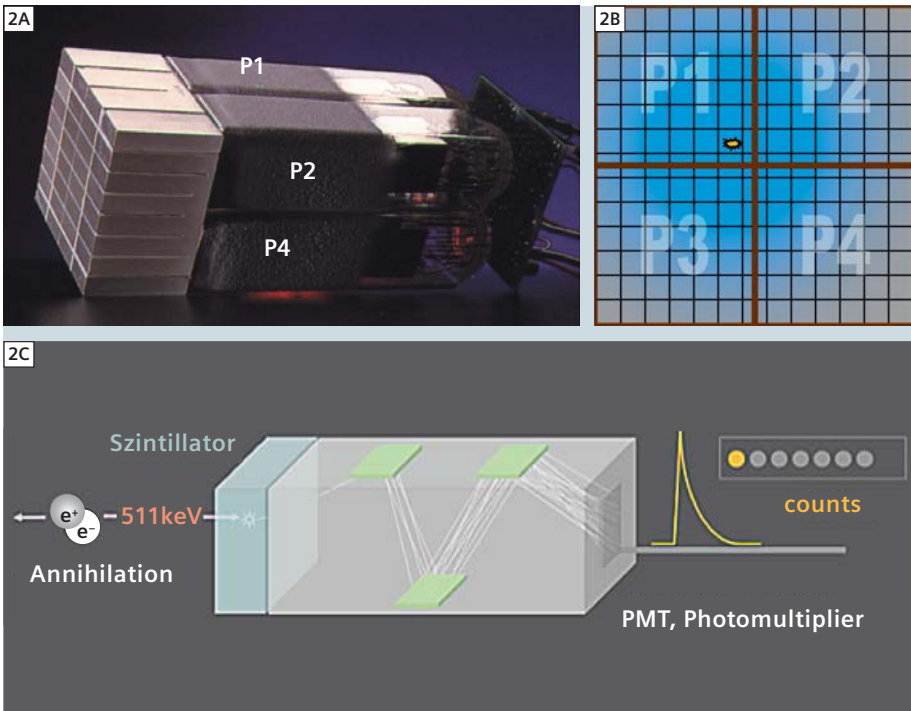
There are a few challenges when designing a PET/CT imaging system and making it clinically viable. First, the axial displacement of the CT and PET components (Fig. 3) is unavoidable as long as no single PET and CT detectors are available, thus allowing for only sequential rather than simultaneous acquisition modes. Sequential imaging holds the risk of involuntary patient motion in between the two examinations and, therefore, may increase the chance of local misalignment of the two studies. Second, residual patient motion is unavoidable in combined PET/CT imaging. Involuntary patient motion from, for example, respiration, cardiac motion, or muscle relaxation leads to PET–CT misregistration that may translate into artifacts on PET images following CT-based attenuation correction. Optimized imaging protocols are required to minimize these types of artifacts and image distortions. Third, the overall exposure from a whole-body PET/CT examination performed with <sup>18</sup>F-FDG is rather high at 20–25 mSv per study and 370 MBq of <sup>18</sup>F-FDG injected. This dose is justified whenever a clinical indication for a combined contrast-enhanced PET/CT study exists, but at the same time it limits the use of PET/CT in selected patients that undergo repeat studies or in subjects for pharmaceutical trials.

Rise of MR/PET

The development of hybrid MR/PET systems started in the late 1990's. CT is not the only available anatomical complement to PET. In comparison to CT, MRI offers a multitude of endogenous contrasts and a superb capa-



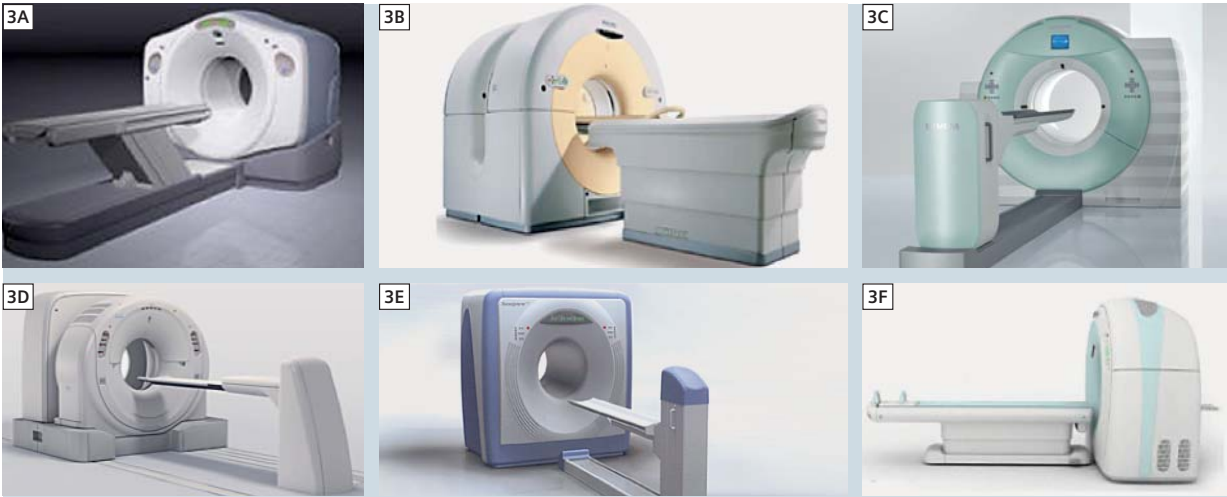
**1** PET is based on the tracing of radioactively labeled metabolites. A radiotracer, e.g. <sup>18</sup>F-FDG (A), is injected into the patient (B): <sup>18</sup>F decays by emitting a positron, which annihilates with an electron, thus resulting in two annihilation photons along a straight line-of-response (LOR), (C) annihilation events are registered in coincidence and stored in raw sinogram space (D). PET images are reconstructed following a number of physical and methodological corrections (E). (Figure adapted from DW Townsend, Singapore.)



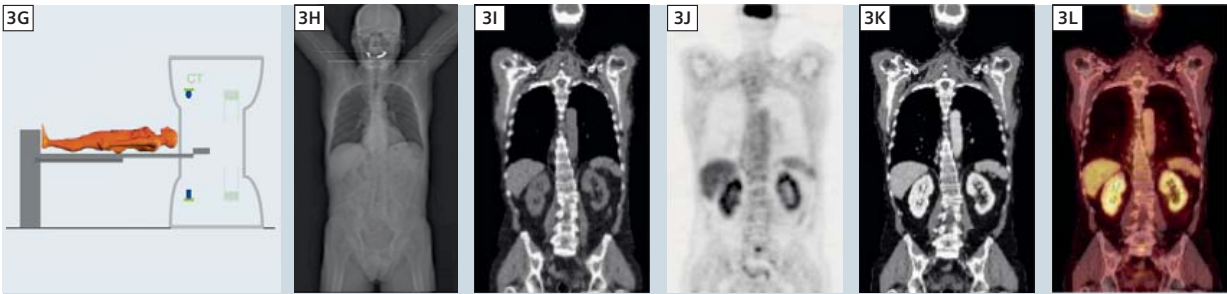
**2** Block detector. (A) Example of PMT-bismuth germanate block detector from a clinical PET system (Fig. 1C). Readout is performed using only the 4 PMTs that are connected to pixelated scintillator block. Light sharing is used to distribute light originating from single pixel between the 4 readout PMTs (P1, P2, P3, P4). (B) Depending on crystal position, scintillation light will be uniquely distributed to readout PMTs. Using Anger weighting algorithm on measured signals, position of incident annihilation photon (i.e. the activated crystal) can be calculated. (C) Schematics of detection process from annihilation to stopping the annihilation photons in the crystal and signal transformation inside the photomultiplier.

bility of differentiating soft tissues. With a sensitivity in the picomolar range, PET is ideally suited for the visualization of specific molecules in living organisms. However, PET lacks the spatial resolution offered by MRI, which in turn lacks sensitivity compared to PET. Therefore, the combination of PET and MRI is highly complementary. MRI also offers anatomical image information with the advantage of causing no risk to the patient from ionizing

radiation and by offering much higher soft tissue contrast than CT, even in the absence of MR contrast agents. But MRI goes beyond plain anatomical imaging. MR spectroscopy, for example, can be used to dissect the molecular composition of tissues by applying selective radiofrequency excitation pulses. The Fourier transformation of the acquired signal provides a spectrum that allows for discrimination between various metabolites.



**3A–F** Current commercial PET/CT systems: (A) Discovery series from General Electrics Healthcare, (B) Gemini series from Philips Healthcare, (C) Biograph mCT from Siemens Healthcare, (D) Acquiduo series from Toshiba Medical Systems, (E) Sceptre series from Hitachi Medical Systems, (F) AnyScan from Mediso (this device can be combined with a SPECT to form a triple-modality imaging system). Variations apply to the individual performance parameters of PET and CT.



**3G–L** Schematic illustration of a standard PET/CT investigation: tracer injection, uptake time and patient positioning (G), topogram and scan range definition (H), CT acquisition for attenuation correction (I), emission scan (J), contrast-enhanced CT scan (K) and image reconstruction/fusion (L).

Spectroscopic images of extended anatomical volumes can be generated for preoperative staging of gliomas, pH imaging, monitoring of temperature, or the evaluation of lactate changes during brain activation. Functional processes in living subjects can also be studied via diffusion-weighted MRI. Here, the magnetic field, generated by different gradients, is used to map phase differences in the MRI signal that are caused by diffusing molecules. Many MRI sequences can be made sensitive to diffusion by using adequate gradient pulses. Diffusion MRI has various potential clinical applications ranging from diagnosing ischemia, cancer, multiple sclerosis, or Alzheimer’s disease to general fiber tracking via diffusion tensor imaging. Diffusion imaging is not restricted to the brain; it has also been applied to other regions of the body (e.g., for oncologic diag-

nosis), where it provides qualitative and quantitative understanding of the tumor microenvironment and the integrity of cell membranes. Functional MRI (fMRI) studies are frequently based on the BOLD (blood oxygen level dependent) effect. This technique is based on the fact that the magnetic properties of oxygenated and deoxygenated hemoglobin in the blood are different and, therefore, produce different signals when imaged with T2\*-sensitive MRI sequences. Unlike contrast-enhanced MRI, BOLD effect is a non-invasive technique based on endogenous information. The BOLD effect also has certain applications in cancer imaging, such as the study of tumor angiogenesis, tumor oxygenation and brain activation in eloquent areas prior to surgical resection. Lately, MRI has become a whole-body imaging modality

thanks to the advent of Tim (Total imaging matrix) and parallel imaging techniques. Image acquisition times have been shortened, thus allowing whole-body MRI examinations with high spatial resolution in less than one hour. Initial results show that whole-body MRI is a promising modality in oncology, especially for the detection of metastases and hematologic malignancies. In summary, MRI holds a great potential in replacing CT as the complementary modality to PET in dual-modality tomographs and in selected indications where MR already outperforms CT.

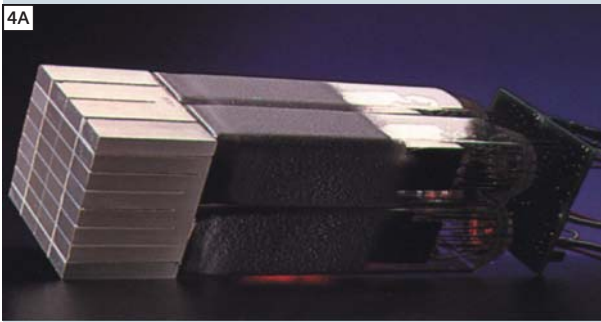
**Challenges of combined MR/PET**

Traditional PET systems use PMTs to detect the scintillation light. However, PMTs are sensitive to magnetic fields and are therefore not functional inside an MRI system. To overcome this problem, various approaches to the combination of PET and MRI have been established. For example, optical fibers can be used to lead the light from the scintillation crystals outside the fringe field of the magnet to the PMTs. Alternatively, split magnets with the PET detector positioned between the two magnet halves and connected via light fibers have been proposed. In either design, long optical fibers result in a loss of light and consequently in lower performance of such a PET system operated in the vicinity of an MR scanner.

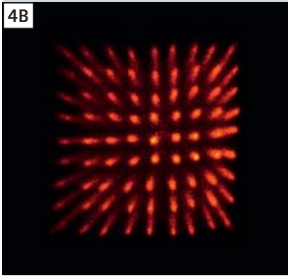
This loss can be overcome by the use of magnetic field-compatible solid state light detectors, such as APDs (Fig. 4). This approach also permits easier expansion of the axial FOV of the PET system. The mutual interference between PET and MR is a critical problem; MR can affect PET performance because of the high static magnetic field, gradient fields, and radiofrequency field. MR image quality, however, can be impaired by either radiofrequency noise introduced by the PET electronics or magnetic field inhomogeneities caused by the presence of different materials in the PET insert and eddy currents induced from the gradient system in the conducting structures of the PET housing and circuit boards. Moreover, the operating temperature needs to be stabilized to ensure reliable PET and MR performance.

Finally, any combined MR/PET system must offer alternative approaches to deriving the necessary attenuation correction factors for the emission data. While in PET/CT attenuation data can be derived from transforming available CT transmission images into maps of attenuation coefficients at 511 keV, no such transmission data are available in MR/PET. This is due to the lack of physical space in general to host a transmission source. Secondly, a rotating metal-encased transmission

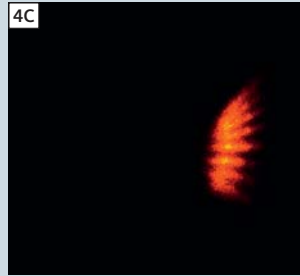
**Conventional PET detectors**



**4A**



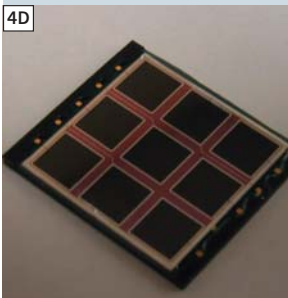
**4B**



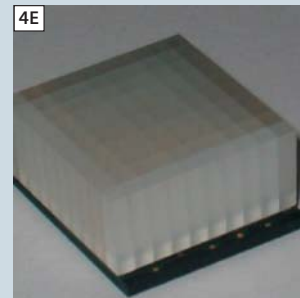
**4C**

$B = 0$   $B \neq 0$

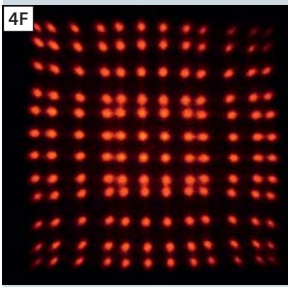
**APD-based PET detectors**



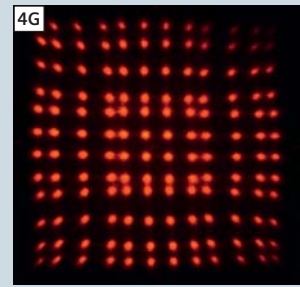
**4D**



**4E**



**4F**



**4G**

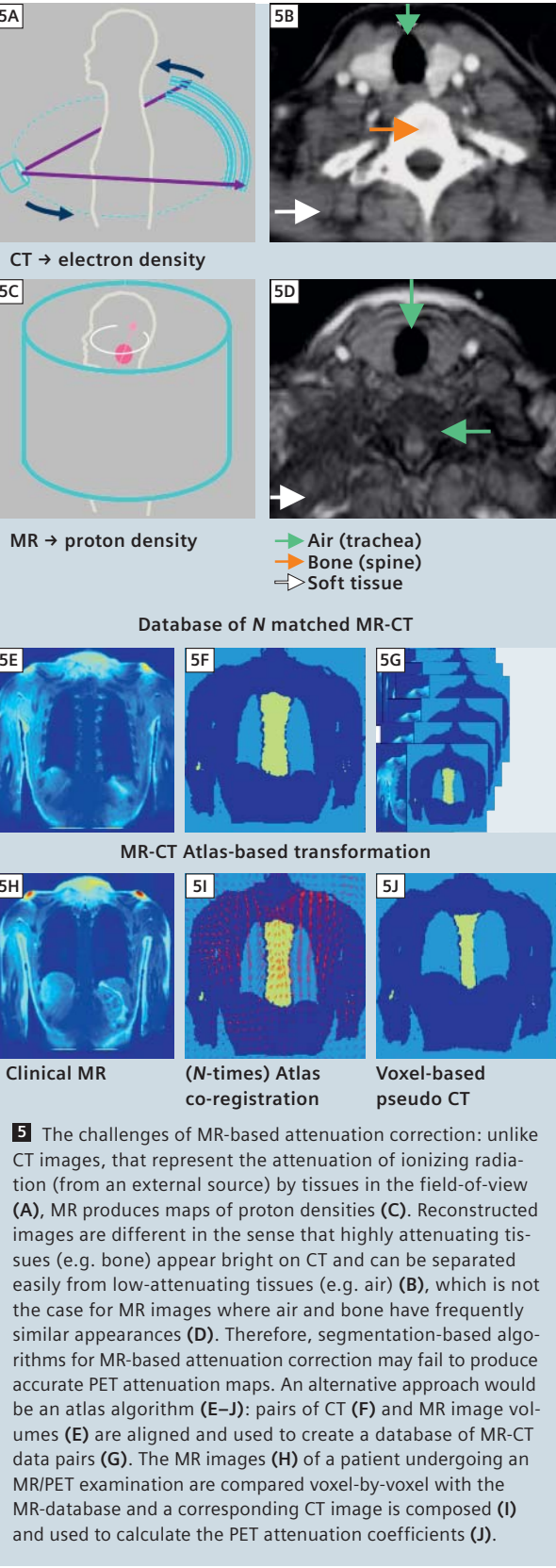
$B = 0$   $B \neq 0$

**4** Conventional PET detectors (A) are based on scintillation crystals and Anger-logics readout. They work only outside magnetic fields (B). If a PMT is operated inside a magnetic field ( $B \neq 0$ ) then the multiplier step is construed and the readout map severely distorted (C). Avalanche photodiodes (APD) based detectors (D, E) are semiconductors that can be operated in magnetic fields, even at ultra-high field strengths (F, G). (Image courtesy of Prof. B. Pichler, University of Tübingen, Germany.)

22 MAGNETOM Flash · 3/2010 · www.siemens.com/magnetom-world

MAGNETOM Flash · 3/2010 · www.siemens.com/magnetom-world 23





source, whether X-ray tube, rod or point sources would lead to grave crosstalk effects with the MR magnetic field. And finally, the available MR images represent, in essence, proton densities that cannot be transformed to maps of electron densities as obtained from CT transmission measurements. Therefore, MR/PET requires novel approaches to MR-based attenuation correction. Segmentation-based approaches have been proposed and seem to work in brain imaging. However, MR-based attenuation correction in extracranial applications is much more demanding (Fig. 5).

Clinical prototype MR/PET

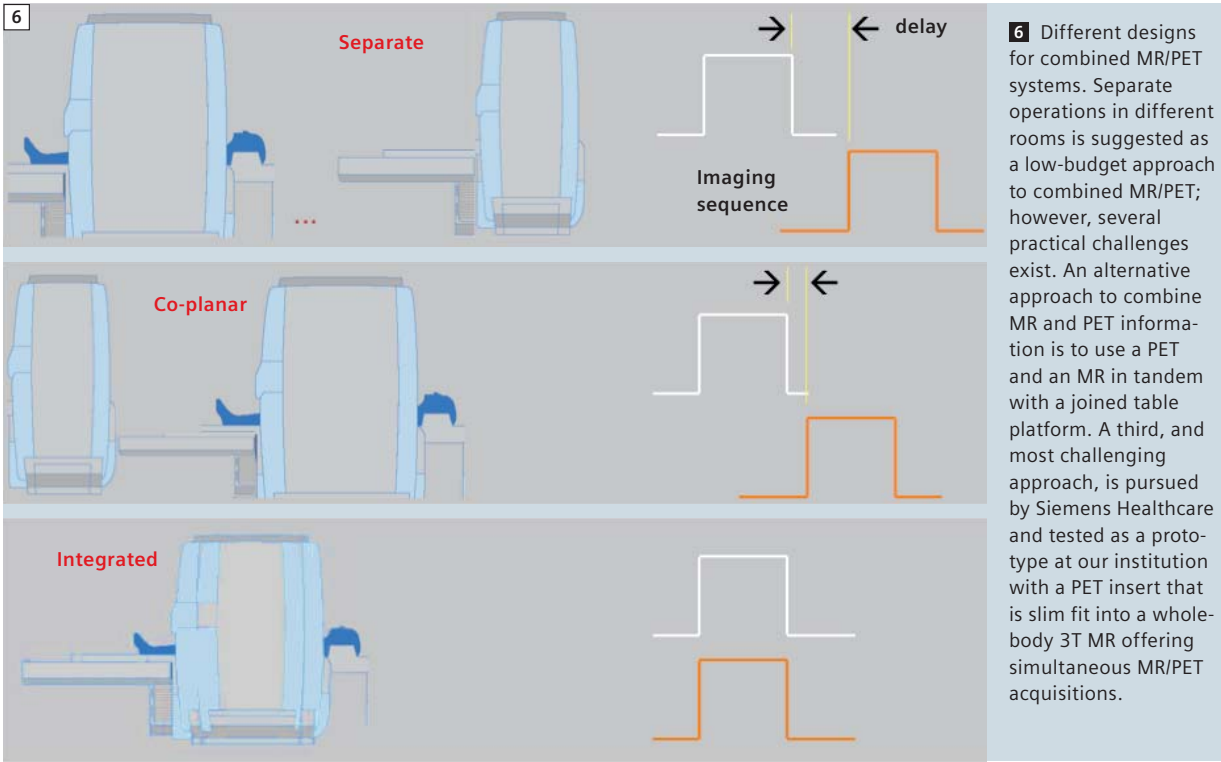
The development of combined MR/PET tomographs has been the reverse experience to that of PET/CT. The first PET/CT design emerged from industry-academia collaboration and was a prototype for human clinical use that stimulated a commercial response and later led to the development of PET/CT for imaging small animals. In contrast, MR/PET in the mid 1990's began with small animal designs.

Then, over a decade later, a prototype MR/PET was developed for human brain scanning that acquired the first images in November 2006. This prototype design is based on a PET insert for a 3T MR, and offers a transverse FOV limited to scanning the brain, or the extremities (Fig. 6). As of today four brain insert MR/PET systems have been installed worldwide; industrial backing for this human MR/PET prototype development is impressive and exceeds that of the early PET/CT developments. This insert design is one of three general approaches to MR/PET being discussed today. An alternative design encompassing a co-axial arrangement of a 3T MRI and a TOF (time-of-flight) PET with a rotating patient handling system in between within one room was proposed in early 2010 (Fig. 6). A comparable system but with separate cabins for MRI and PET has been in existence for brain research since 2007. Again, several prototype systems were installed for clinical testing. A third, much simpler approach is also illustrated in figure 6. While the integrated MR/PET is the most sophisticated and perhaps ideal solution to combined imaging, the third design is that of a standalone PET and a standalone MR with a unified table docking station.

First experiences with MR/PET

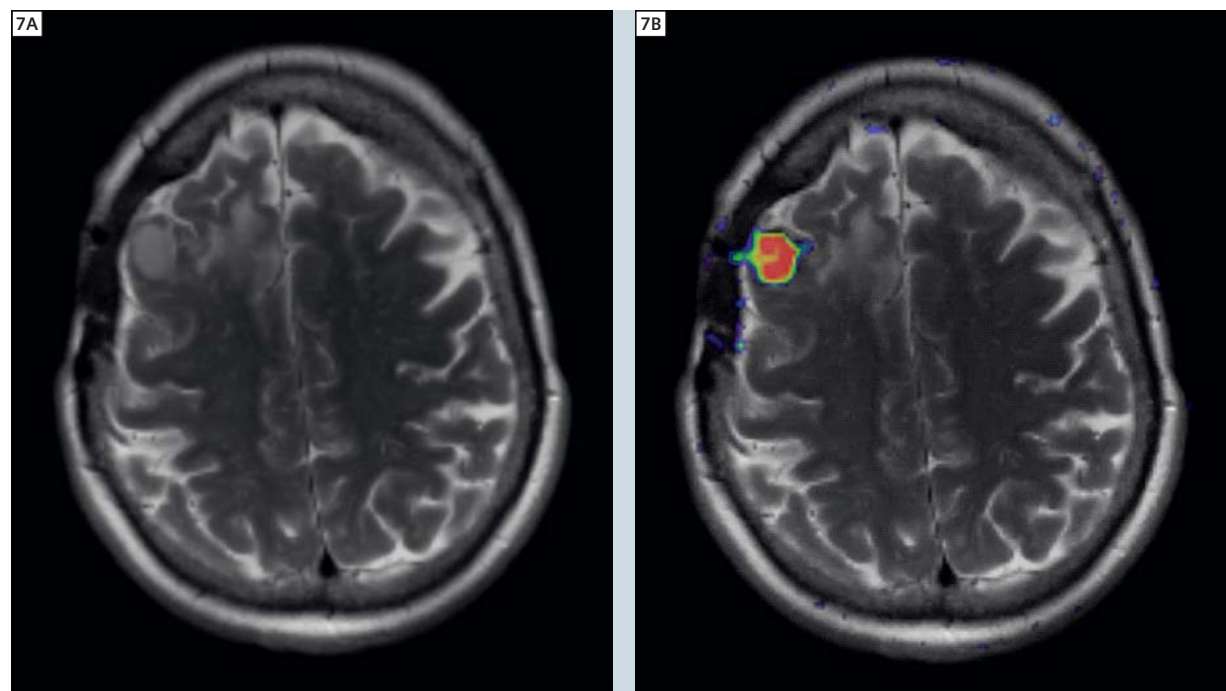
First results of clinical simultaneous MR/PET

We received a prototype MR/PET system in 2008 and have evaluated the system since then. Our patient studies, as approved by the Ethic Committee, aim at demonstrating the feasibility of simultaneous MR/PET imaging of the human brain by using APD-based PET



detector technology integrated into a clinical 3T MAGNETOM Tim Trio system. The PET system consists of blocks of a 12 x 12 LSO matrix with an individual crystal size of 2.5 x 2.5 x 20 mm<sup>3</sup>. The block is displayed on a 3 x 3 APD array with individual diodes that have an active surface of 5 x 5 mm. Six LSO-APD block detectors form a cassette; the cassettes are arranged along the z (main) axis of the tomograph, thus forming 72 crystal rings. The entire PET system consists of 32 radially arranged cassettes and has an axial FOV of 19.2 cm and an inner ring diameter of 35.5 cm. The system has a time resolution of 5.6 ms (full width at half maximum, FWHM) and a mean energy resolution at 511 keV of 22% (FWHM). All PET detector components such as amplifiers, resistors, shielding material and housing were selected to minimize interference with the MR imaging B field, gradients, and radio-frequency. MR examinations are performed during PET data acquisition. Conventional MR imaging of the brain includes axial T2-weighted turbo spin-echo (TSE), fluid-attenuated inversion recovery sequence (FLAIR) and 3D T1-weighted fast low-angle shot sequence (FLASH) sequences. For diffusion-weighted imaging (DWI), a single-shot echo-planar imaging (SS-EPI) sequence is applied.

For PET imaging, the patients fast for at least 4 hours prior to the intravenous injection of <sup>18</sup>F-FDG. Body-weight adjusted, we inject in mean 370 mBq of <sup>18</sup>F-FDG. The distribution of the tracer is recorded during the entire MRI acquisition (time-range for simultaneous MR/PET from 20 to 40 minutes in most cases) at a steady state at 120 min post injection. The extended uptake time is due to the fact that all patients first undergo a clinically indicated PET/CT. PET data are acquired in 96-bit list mode containing complete information for each coincident event and stored on a disk, accumulating approximately 20 GB of raw data during a 40 min of PET acquisition. Emission data set is reconstructed iteratively (6 iterations and 16 subsets). The image volume consists of 153 transaxial image planes with a voxel size of 1.25 mm<sup>3</sup>. Reconstructed resolution is 2.5 mm (FWHM) in the center and 4.5 mm at 10 cm off axis (for a line source in air reconstructed by using OPOSEM3D). Our experience and studies indicate that – following system set-up and quality control - simultaneous MR/PET of intracranial tumors using <sup>18</sup>F-FDG, <sup>11</sup>C-methionine or <sup>68</sup>Ga-DOTATOC can be performed reliably. The image quality and quantitative data achieved using MR/PET is similar to that using PET/CT. An example MR/PET study is shown in Figure 7.



**7** MR/PET imaging of a 65-year-old patient with a meningioma in the right frontal lobe. **(A)** Axial T2w MR images. **(B)** The intrinsic fusion of the simultaneously acquired MR and  $^{68}\text{Ga}$ -DOTATOC PET images highlights the advantage of hybrid imaging regarding the accurate spatial coregistration without distorting artifacts. Data have been acquired using the integrated BrainPET MR/PET system (Siemens Healthcare, Erlangen, Germany).

The development of a prototype integrated MR/PET imaging system with no detrimental effect on the performance of PET and no degradation of MR images for a number of standard clinical MR images has put MR/PET imaging on the verge of being applied to clinical neurosciences. The combined system will certainly broaden the impact and possibilities of simultaneous imaging of morphologic, functional and metabolic information. First patient data are promising and highlight the scientific and clinical potential of the integrated system.

#### Challenges of (simultaneous)

##### MR/PET: Quantification

Together with the clinical and performance evaluation of the prototype MR/PET at our hospital, we have initiated the development of versatile approaches to MR-based attenuation correction (AC) for clinical use. Performing PET attenuation correction with MR image information is challenging. Various approaches for predicting the attenuation maps from MR images have been proposed by several groups. MR image segmentation works well for the brain but can fail on extra-cerebral images, mainly due to the similar appearance of air and bony tissues as well as artifacts towards the edge

of the FOV of MR images. If a separation of bone and air is required, torso MR/PET imaging in particular requires more sophisticated methodologies. We focus on a combination of an atlas approach and machine-learning algorithm to estimate a PET attenuation map from the available MR images (Fig. 5), which was shown to work well in our hypothesized whole-body MR/PET data. In general, MR-AC must address adequate transformation of MRI pixel value information to appropriate PET attenuation values and account for additional pitfalls, such as truncation effects from patients extending beyond the transverse FOV of the MR system and the presence of MR surface coils typically not seen on MR imaging. In latter cases, dedicated MRI sequences using ultra-short echo times appear as promising adjuncts to MR imaging for the purpose of MR-AC.

##### Challenges of simultaneous MR/PET: workflow

In terms of workflow aspects and logistics, integrated imaging techniques – in theory – can outperform any separate or sequential imaging. This has direct implications on patient comfort and compliance. Nonetheless, a number of questions remain with respect to the overall integration of this new combined modality into clinical workflow, be it as an adjunct or as a

replacement method; this needs to be addressed by prospective studies. In the interim there are indications for numerous research applications that benefit from simultaneous MR/PET imaging, currently for brain application only, in the near future for larger imaging areas. Simultaneous imaging functionalities must comprise hardware and software tools. As hardware integration of the combined system progresses, so must the integration with respect to software and data processing. Current viewing tools need to be expanded to allow efficient screening, accurate analysis and quantification, where needed, of data sets that comprise 3D images, dynamic data and additional information, such as spectra, perfusion maps or multiple metabolic pathways.

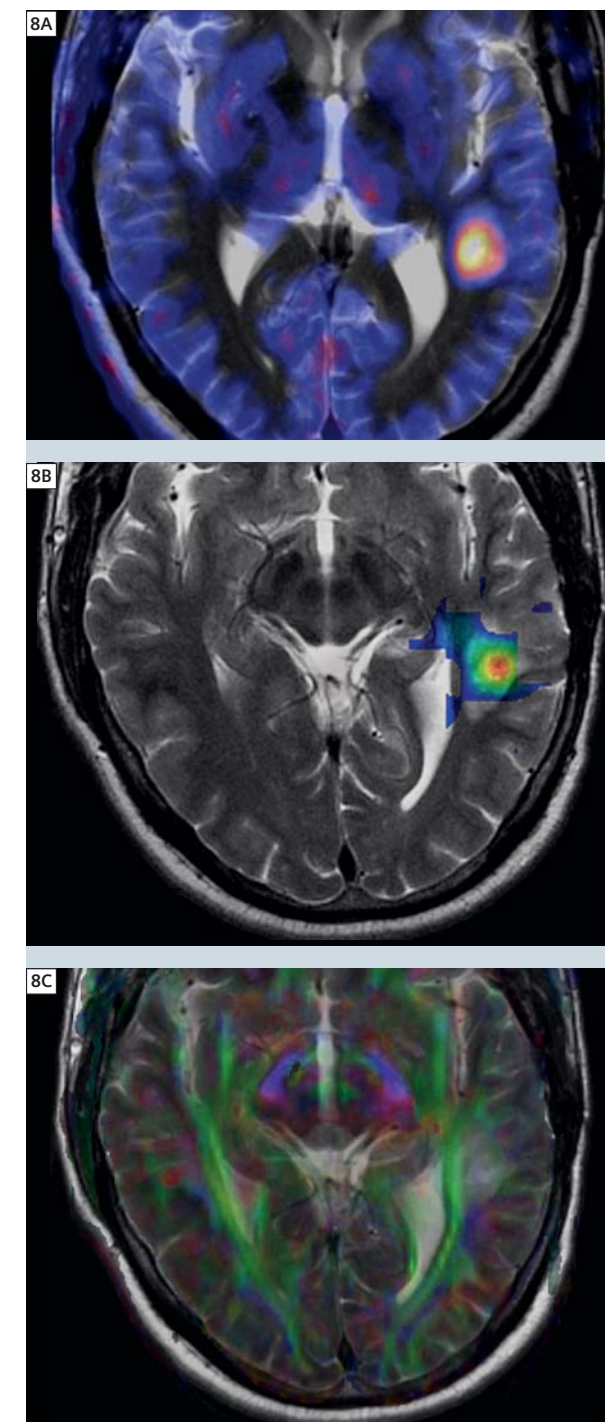
#### Simultaneous versus sequential MR/PET imaging

It may be too early to predict a prevalence of one over another acquisition mode. The question of sequential over simultaneous imaging is the subject of an ongoing debate. From a technical perspective simultaneous imaging allows for a number of advanced data processing steps that are not straight forward in sequential MR/PET (and PET/CT imaging). This includes motion correction for involuntary patient motion and any subsequent quantification that may be biased from patient motion during the examination. MR-based motion correction is work-in-progress.

To correct for patient motion, special MRI sequences can be applied by either 1-dimensional navigator scans or in 2 to 3 dimensions to detect the motion of the subject. Ideally, these protocols can be combined with the MRI sequence already running to provide motion information about the subject in intervals of as short as 1 s. The motion vectors may be extracted from the motion-sensitive MRI scans and made available to the PET system, allowing either online or post acquisition motion correction of the PET images. General advantages of simultaneous data acquisition include temporal correlation of PET and MR imaging data, reduced imaging time compared with sequential imaging, and the option for cardiac and respiratory motion correction of PET data.

#### MR/PET – What can be expected in the near future?

With the success of PET/CT in mind, the expectations for any new combination, such as MR/PET are very high. Obviously, MRI provides excellent soft tissue contrast without using ionizing radiation. Thus, it seems a perfect anatomical complement to PET (Table 1). The main idea behind merging PET and MRI is to combine the functional / metabolic information provided by PET with the high soft-tissue contrast and the func-



**8** Simultaneously acquired and superimposed on  $^{11}\text{C}$ -methionine-PET and MR imaging avid tracer uptake of the atypical neurocytoma on the left side in a 42-year-old patient **(A)**. Simultaneously acquired chemical shift imaging (CSI) MR spectroscopy provides a map of choline to N-acetyl-aspartate ratio **(B)** indicating the high proliferating index of the tumor, while simultaneous diffusion tensor imaging **(C)** shows the clear relationship to the adjacent optic radiation.



tional information offered by MRI. However, the potential areas of application of combined MR/PET extend far beyond high-contrast image fusion. This is supported by our in-house studies where the pre-clinical and clinical prototypes have convincingly demonstrated that the APD-based PET system can be operated simultaneously with the MRI without sacrificing the performance of either modality.

Brain studies, for example, benefit greatly from the additional morphologic information provided by MRI. Simultaneous data acquisition will allow the addition of kinetic, functional and metabolic information for real time multi-parametric functional imaging; to name just two applications:

- MRS can provide additional metabolic information to regional metabolic data from PET in stroke, gliomas, and degenerative disorders;
- MR-based perfusion-weighted imaging (PWI) can be correlated with hypoxic markers (<sup>18</sup>F-MISO PET) for correcting PET results and also for further understanding of tumor microenvironment.

For complex studies of brain functions combinations of modalities or additional functional techniques will open new insights into the organization of the brain and the changes in disease. For example, diffusion tensor imaging can be added to activation studies and therefore, effects on transmitter release, receptor occupancy and metabolism in connected areas can be analyzed as substrates of connectivity in networks (Fig. 8). The list of conceivable research topics and clinical applications of MR/PET is extensive. It could be particularly useful for early tumor detection and functional

therapy monitoring in oncology. It will likely be used to investigate the effect of novel drugs, such as inhibitors of angiogenesis or modulators of the immune system. Integrated information on individual cell metabolism and microenvironment and their response to therapy will help elucidate the mechanism of action and optimize treatment schedules.

In the field of cardiology, the potential of MRI to assess cardiac function can be combined with the possibilities offered by cardiac PET; this combination would allow clinicians to assess the metabolic viability of the heart muscle, its perfusion and functional impairment. Initial studies combining MR spectroscopy with PET have already been performed on isolated perfused rat hearts, but may also elaborate cardiac MR/PET studies involving cardiac stress simultaneously assessed with PET and MRI. Dual functional studies correlating the same parameters (e.g. perfusion in PET via radioactive water or ammonia and in MRI using arterial spin labeling or MRI contrast agents) can help to cross correlate and validate different acquisition techniques. Using the strengths of each individual modality, one can simultaneously assess different molecular parameters. For instance, diffusion processes may be tracked simultaneously with PET tracer uptake, or PET perfusion can be correlated with the MRI BOLD effect. Because of the large number of existing PET probes and the various functional imaging capabilities of MRI, the number of possible combinations for molecular imaging readouts is virtually unlimited. The advantage of truly simultaneous MR/PET is that the same subject is scanned at the same time with identical environmental parameters and stimuli. It is

likely that such functional studies will further push the limits for basic biologic research and will open new realms for studying biology in vivo.

Finally, applications of MR/PET imaging in oncology are likely to expand. Recent clinical studies comparing whole-body MRI and PET/CT have indicated the potential advantages of a combination of MR and PET. The superior soft tissue contrast of MR is in general relevant for all types of soft tissue tumors regarding detection, delineation, characterization, and staging. Nonetheless, CT is still more sensitive than MR in revealing smallest lung nodules. On the other hand, dynamic MR studies that yield various parameters for quantification of perfusion without additional radiation exposure, and PET studies that may be performed simultaneously visualize in whole the tissue and the vascular components of the tumor.

One of the primary strengths of MRI is its ability to provide anatomical detail in addition to detect abnormalities within boney structures (e.g. marrow, joint spaces). <sup>18</sup>F-FDG PET is useful in the diagnosis of acute infections and is an accurate imaging modality to exclude the diagnosis of osteomyelitis. When combined and clinically available, MR/PET may provide a more accurate diagnosis of patients with osteomyelitis including those with complicated diabetic foot disease.

The complementary morphological and metabolic data can be relevant for defining biopsy targets, particularly by differentiating areas of active tumor involvement from inflammatory disease, fibrosis or necrosis. Combined morphological and metabolic imaging is also important for the evaluation of early treatment response. Metabolic information assessed e.g. by <sup>18</sup>F-FDG (marker for glucose consumption and therefore energy consumption) or <sup>18</sup>F-FLT (fluorothymidine; marker for nuclide acid synthesis and therefore proliferation) is more sensitive for detecting therapy-induced metabolic and necrotic tissue damage. Additional high-resolution morphologic information may be potentially helpful in the planning of subsequent surgery and radiotherapy.

A decade of hybrid imaging

A mere two years after the advent of commercial PET/CT, Johannes Czernin from UCLA commented: “PET/CT is a technical *evolution* that has led to a medical *revolution*”. Today, at the dawn of MR/PET imaging, we may extend his phrase by “integrated MR/PET is a medical *evolution* based on a technical *revolution*”. PET/CT appears to have replaced stand-alone PET for nearly all oncologic indications. Ongoing and future studies using first prototype and clinical systems will

show how much MR/PET could supplement PET/CT imaging in the clinic. We believe that MR/PET is a required and valuable adjunct to modern healthcare and that there will be indications for which MR/PET may become a primary or secondary diagnostic test during work-up or follow-up of a variety of patients. Nevertheless, MR/PET will not replace PET/CT as a molecular imaging modality in the near future. Both modalities are here to stay because both platforms incorporate the diagnostic power of PET. In fact, with PET/CT being a “*dual*-modality imaging” platform by virtue of combining functional (PET) and anatomical (CT) imaging only MR/PET offers true “*multi*-modality imaging” by virtue of combining function (PET) and anatomy and function (both MR). This will open, without a doubt, new avenues in non-invasive imaging as part of clinical patient management and clinical research.

**Contact**  
Thomas Beyer, Ph.D.  
Imaging Science Institute (ISI) Tübingen  
University Hospital Tübingen  
Dept. of Diagnostic and Interventional Radiology  
Hoppe-Seyler-Str. 3  
72076 Tübingen  
Germany  
Tel.: +49 7071 29 81212  
thomas.beyer@cmi-experts.com

<http://health.siemens.com/isi/index.php>  
[http://health.siemens.com/isi/index\\_eng.php](http://health.siemens.com/isi/index_eng.php)

Table 1: Assessment of biological properties by MR and PET.	
MR	PET
Morphology	Flow (H <sub>2</sub> <sup>15</sup> O)
Water diffusion capacity (DWI)	Metabolism ( <sup>18</sup> F-FDG)
Vascular anatomy (MRA)	Blood volume (C <sup>15</sup> O)
Perfusion (PWI, DCE-MRI)	Oxygen consumption ( <sup>15</sup> O)
Tissue metabolites (MRS)	Hypoxia ( <sup>18</sup> F-MISO)
Functional activation (fMRI)	Vascular permeability (labeled AA)
Cerebral fiber tracts (DTI)	Nuclide acid synthesis ( <sup>18</sup> F-FLT)
Oxygen consumption ( <sup>17</sup> O)	Transmitters (e.g. <sup>18</sup> F-DOPA)
Migration of cells (Fe labeling)	Enzymatic activity (e.g., MP4A)
	Angiogenesis (e.g. <sup>18</sup> F-RGD)
	Distribution and kinetics of tracers and drugs (labeled compounds)
	Enzymatic activity in transfected cells

# T<sub>1</sub>-weighted DCE Imaging Concepts: Modelling, Acquisition and Analysis

Paul S. Tofts, PhD

Brighton and Sussex Medical School, Falmer, Sussex, United Kingdom

## 1. Introduction

There are increasing opportunities to use Dynamic Contrast-Enhanced (DCE) T<sub>1</sub>-weighted imaging to characterize tumor biology and treatment response, using the modern fast sequences that can provide good temporal and spatial resolution combined with good organ coverage [1]. Quantification in MRI is recognized as an important approach to characterize tissue biology. This article provides an introduction to the physics concepts of mathematical modelling, image acquisition and image analysis needed to measure aspects of tumor biology using DCE imaging, in a way that should be accessible for a research-minded clinician.

Quantification in MRI represents a paradigm shift, a new way of thinking about imaging [2]. In qualitative studies, the scanner is a highly sophisticated camera, collecting images that are viewed by an experienced radiologist. In quantitative studies, the scanner is used as a sophisticated measuring device, a scientific instrument able to measure many properties of each tissue voxel (e.g. T<sub>1</sub>, T<sub>2</sub>, diffusion tensor, magnetisation transfer, metabolite concentration, K<sup>trans</sup>). An everyday example of quantification would be the bathroom scales, used to measure our weight. We expect that the machine output shown on the dial, in kg, will be accurate (i.e. close to the true value), reproducible (i.e. if we make repeated measurements over a short time they will not vary), reliable (the scales always work) and biologically relevant (the quantity of weight does indeed relate to our health). An example of a clinical measurement would be a blood test; we expect it to work reliably every time. This is the aspiration for quantitative MRI: that it should deliver a high quality measurement that relates only to the patient biology (and not the state of the scanner at the time of measurement).

The transfer constant K<sup>trans</sup> (see below) characterizes the diffusive transport of low-molecular weight Gd chelates across the capillary endothelium [3]. It can be

measured using DCE MRI, and has been widely used in imaging studies to characterize tumor biology and treatment response. The fractional volume v<sub>e</sub> of the extravascular extracellular space (EES; i.e. the interstitial space), can also be measured. A consensus recommendation [4] proposed that in assessing anti-angiogenic and anti-vascular therapies, K<sup>trans</sup> should be a primary endpoint. Secondary endpoints should include v<sub>e</sub>, the rate constant k<sub>ep</sub> (k<sub>ep</sub>=K<sup>trans</sup>/v<sub>e</sub>) and the plasma volume v<sub>p</sub> (if available). The traditional clinical evaluation of tumor treatment is the RECIST criterion, based on tumor diameter; however a tumor could die but not shrink, and K<sup>trans</sup> and v<sub>e</sub> may often be more sensitive markers of tumor metabolism. There are also applications of DCE-MRI in tissues other than tumors, e.g. renal and myocardial function; this article focuses on tumor applications, with one example of renal function.

## 2. MRI modelling

Before any pharmacokinetic analysis can take place, the Gd contrast agent (CA) concentration has to be found from the MRI signal enhancement. This requires an MRI model, which has two components. First, T<sub>1</sub> is reduced by the presence of CA (eqn. 1 see appendix). The relaxivity r<sub>1</sub>, (i.e. the constant of proportionality between Gd concentration and increase in relaxation rate R<sub>1</sub>=1/T<sub>1</sub>) is usually assumed to be equal to the in-vitro value (measured in aqueous phantoms), although it can alter in-vivo. The native T<sub>1</sub> of the tumor (i.e. the value before injection of CA, T<sub>10</sub>) must also be known. Second, the way in which the T<sub>1</sub> reduction increases the signal is modelled (eqn. 3); this is specific to each sequence type, and also requires accurate knowledge of the flip angle FA. The most common sequence is the simple gradient echo (FLASH), on account of its speed; the sequence must be truly spoiled (i.e. there is no build up of steady state transverse magnetisation). Provided

these 3 parameters (r<sub>1</sub>, T<sub>10</sub>, FA) are known then there is a clear relationship between signal and Gd concentration.

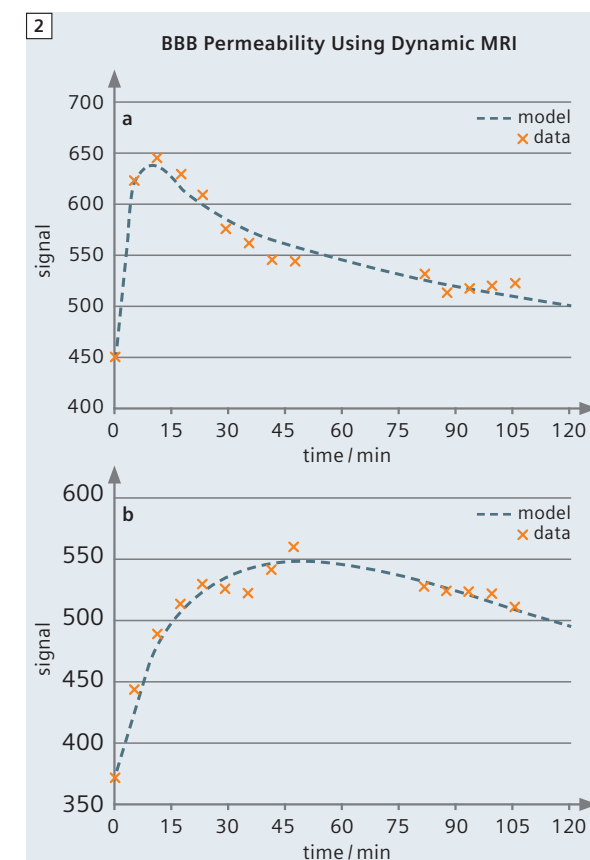
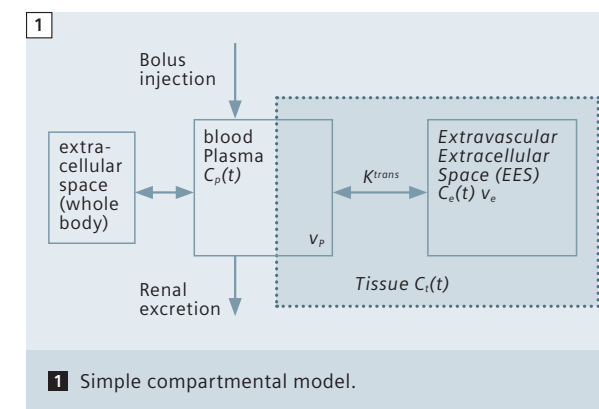
Some studies attempt to find Gd concentration from signal by using a phantom calibration curve; however these approaches are usually flawed, since the signal is also proportional to proton density (which is greater in an aqueous solution than in tissue), and the FA may be different when imaging the phantom (caused for example by different coil loading or B<sub>1</sub> inhomogeneity). The plasma concentration (required for the pharmacokinetic modelling – see below) may be measured from the blood signal. In this case, blood concentration is first found from the blood signal (using eqn. 3). The plasma concentration is about 70% higher, once haematocrit is taken account of (eqn. 4).

## 3. Pharmacokinetic modelling

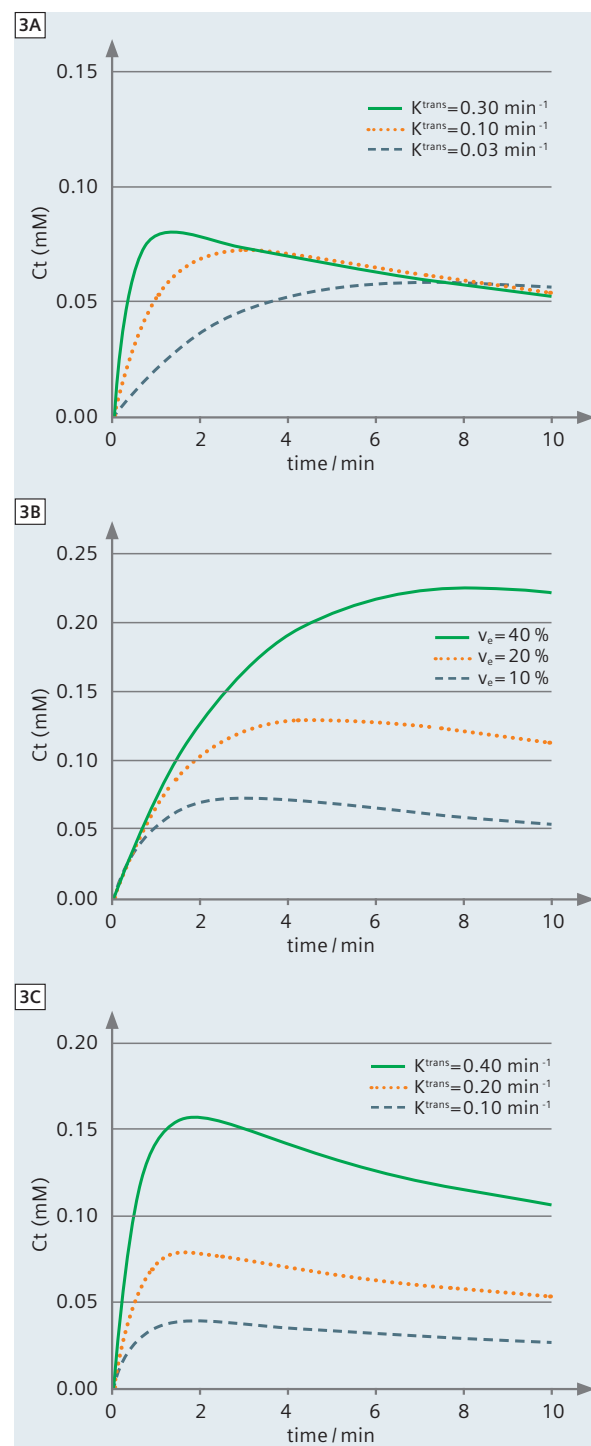
Given the Gd concentration as a function of time, pharmacokinetic analysis can now be undertaken to model how the CA distributes in the body, and how this depends on characteristics of the tumor biology. This is independent of the imaging conditions (MRI field strength etc.), and in principle even independent of imaging modality (CT or MRI). Most modelling uses the concept of a compartment; this is like a bucket: the Gd tracer inside is dissolved in water and at the same concentration everywhere, and the flow into or out of the bucket is small enough to allow the contents to remain well mixed.

The simplest compartmental model has one tissue compartment in addition to a vascular compartment; the so called 'Tofts model' [5] (mathematically equivalent to that proposed by Kety [6] in a non-MRI context), used to measure K<sup>trans</sup> and v<sub>e</sub> (see fig. 1). The bolus injection of Gd gives a time-varying blood plasma concentration C<sub>p</sub>(t), which can be measured in each subject, or else a population average can be used. Since the commonly used contrast agents are small (<≈ 1000 Daltons) then the leakage from the capillaries into the EES is diffusive and hence reversible; it is therefore proportional to the difference in concentrations, and K<sup>trans</sup> is the constant of proportionality (eqn. 5). The total Gd concentration in a voxel or ROI (eq 6) is the sum of the EES contribution (which usually dominates, since v<sub>e</sub> ≈ 10–60%) and the intravascular contribution (the 'vp term') which is often small and ignored (v<sub>p</sub> ≈ 1–10%) [7].

This model was able to explain signal enhancement in multiple sclerosis lesions [5] (fig. 2), and gave values of K<sup>trans</sup> and v<sub>e</sub> consistent with the known biology of acute and chronic lesions.







**3** Simulations of tissue concentration after bolus injection of 0.1 mmole/kg of Gd, for a range of  $K^{trans}$  and  $v_e$  values, ignoring any IV contribution.

(A) Increasing  $K^{trans}$ , with fixed  $v_e = 10\%$ .

(B) Increasing  $v_e$ , with fixed  $K^{trans} = 0.1 \text{ min}^{-1}$ .

(C) Constant  $k_{ep} = 2 \text{ min}^{-1}$ , increasing  $K^{trans}$ .

The differences in enhancement curve shape, and the time of peak enhancement, both apparent in fig. 2, are important. A model simulation [5] using typical  $K^{trans}$  values for tumors shows that the initial slope depends on  $K^{trans}$  (fig. 3A), and is independent of  $v_e$  (fig. 3B).

The final peak value depends on  $v_e$ , and larger  $v_e$  tumors take longer to reach their peak (fig. 3B). The shape of the curve is determined by  $k_{ep}$ , and if  $K^{trans}$  is increased whilst keeping  $k_{ep}$  fixed, the curve increases in amplitude but retains the same shape (fig. 3C) as is expected from equation 6.

In the original formulation of the model (applied to multiple sclerosis), trans-endothelial leakage was low enough that there would not be significant local depletion of Gd concentration in the capillary. Perfusion  $F$  was sufficient to maintain the capillary concentration at the arterial value. In this case,  $K^{trans}$  is just the permeability surface area product (PS), and DCE could reasonably be called 'permeability imaging'. This 'permeability-limited' case is defined by  $F \ll PS$ . In tumors, the endothelium can be much more leaky, there may be local depletion, and  $K^{trans}$  will represent a combination of permeability and perfusion [3]. In the limiting case of very high permeability, then  $K^{trans}$  will equal perfusion, and DCE could reasonably be called 'perfusion imaging'. This is the 'flow-limited case', defined by  $F \gg PS$ .

The modelling of the capillary vasculature shown in figure 1 is naive, and not surprisingly at high temporal resolution it fails. Modern sequences can sometimes provide a temporal resolution of  $\sim 1 \text{ s}$  (depending on the organ and the coverage required), and in these cases the initial rise in signal gives information about perfusion, as Gd arrives in the capillary bed over a few seconds. More sophisticated models are then able to extract pure perfusion information [8, 9], and potentially pure permeability information as well. In DCE kidney imaging, the perfusion peak in tissue is clearly delayed (by about 4 s) with respect to the arterial peak (see fig. 5).

#### 4. Image acquisition

In DCE imaging, repeated  $T_1$ -weighted images are collected for several frames before Gd is injected, and then for several minutes afterwards. This is often preceded by a  $T_1$  measurement. A good bolus injection can be achieved by using a power injector, with a saline flush after the Gd. The receiver gain must be controlled for the whole series of DCE images.

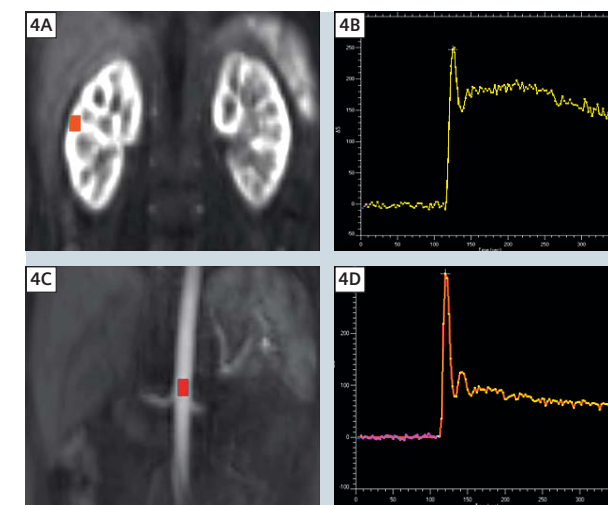
Quality assurance [2] can be used to ensure the scanner is stable for the DCE acquisition period. Either a phantom can be repeatedly imaged (this can also be used to check  $T_1$  accuracy), or a volunteer can be repeatedly scanned (without Gd).

The sequence parameters will involve compromise between coverage, temporal resolution and spatial resolution. Newer scanners have faster gradients (allowing shorter TR's), and multi-array receive coils give higher SNR at short TR's. The optimal sequence will depend on the organ being measured; often frame times of 2–20 s can be achieved. 3D (volume) sequences are preferred, since they have better FA accuracy than 2D (slice selective) sequences. Body coil transmission gives better FA accuracy than combined transmit/receive coils. In the abdomen, a coronal-sagittal oblique slice orientation (instead of transverse) has two advantages: the aorta can be sampled along its length, removing wash-in effects, and breathing movement is mostly in-plane and therefore more easily corrected.

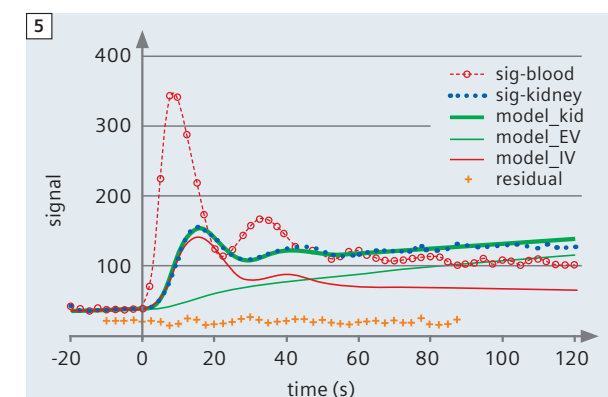
The blood curve may be measured, in order to provide an AIF for the modelling. In this case a temporal resolution of  $\sim 3 \text{ s}$  or less is desirable, and it is usually the aorta that is imaged. Wash-in effects are reduced by ensuring that the blood is fully saturated (i.e. has experienced several RF pulses) by the time it reaches the location of the region of interest (ROI).

The DCE sequence should ideally be run long enough to sample the enhancement plateau. If not, then  $v_e$  cannot be reliably measured, since it does not affect the rising part of the curve, only the plateau value (see fig. 3B). An example of rapid DCE is shown in figure 4. Imaging of the kidney and aorta at a temporal resolution of 2.5 s, using half standard dose of Gd, allows the perfusion phase of the tissue signal to be seen, and it has a clear delay with respect to the aortic peak. In this organ the blood volume is large (about 30%), and can be estimated because the perfusion peak is so distinct. A modified model fits the data well (fig. 5); in this model of the uptake phase (up to 90 s), the vascular delay and dispersion are accounted for, and there is no efflux from the parenchymal ROI. Renal filtration occurs mostly after bolus passage, and can be well estimated. GFR estimates in controls are in good agreement with normal values (reference 10 and manuscript in preparation). There is scope to optimise the FA. A small FA gives more signal at low concentration, but has limited dynamic range (see fig. 6 FA = 5°); increasing the FA gives increased sensitivity to Gd (fig. 6 FA = 10°); further increases (fig. 6 FA = 20° or 30°) give a wider dynamic range (at the expense of reduced sensitivity) and are needed if measuring the AIF (peak blood concentration 6mM [11] and see fig. 7 below) as well as tissue enhancement. Nonlinearity is not a concern as it is properly dealt with in the MRI model.

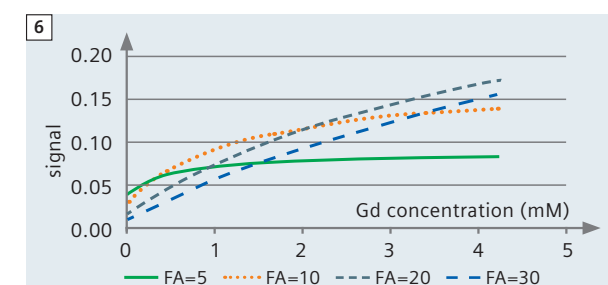
Breathing causes serious artifacts in body imaging. There are several approaches to minimising its effect:



**4** Signal enhancement in kidney and aorta. A cortical ROI (A) is used to define the time of peak enhancement (B) and hence the arterial ROI (C) giving the blood curve (D).



**5** Model analysis of renal enhancement. The kidney signal (sig-kidney) is clearly delayed (by about 2 time points) from the blood signal (sig-blood). The model fit (model-kid) shows separately the extravascular filtered Gd (model-EV, from which GFR is found) and the intravascular Gd (model-IV, from which blood volume and perfusion are estimated).



**6** Performance of gradient echo sequence with various FA values. Eqns 2 and 3 were used, with TR = 3 ms;  $T_1 = 1 \text{ s}$ .

- i) Allow free breathing and minimise diaphragm movement by having hands above the head. This can be uncomfortable; having a single hand above the head is easier and nearly as effective.
- ii) Breath-hold for first pass (~20 s) then allow breathing (although this can result in a large movement as breathing resumes).
- iii) Free breathe and discard data at the extremes of position (using the images or respiratory monitoring to detect the extrema).
- iii) Guided free breathing (instructions from the imaging radiographer).

Whether breathing should be controlled or not is currently unclear (this may depend on the kind of patient, and the availability of registration – see below), and is the subject of ongoing research.

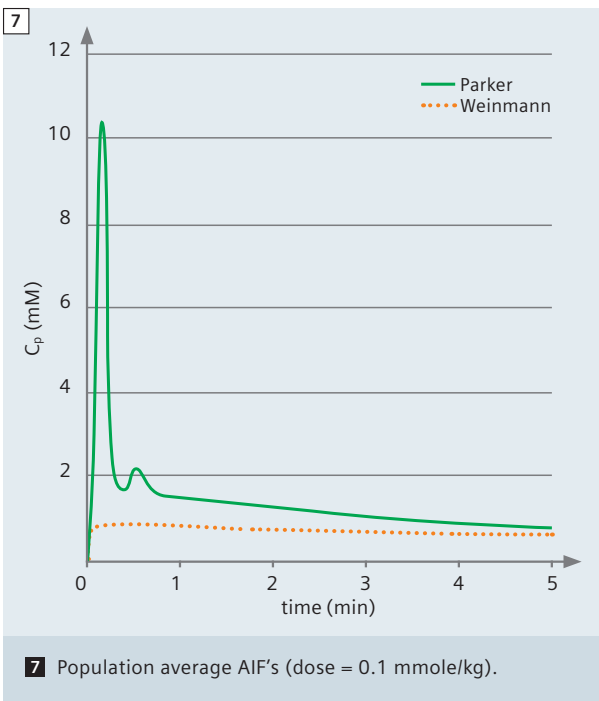
Flip angle accuracy is often poor yet crucial in determining the accuracy of the  $K^{trans}$  value. It affects the calculation of concentration from enhancement (eq. 3), the estimation of the AIF, and the measurement of  $T_{10}$ .  $B_1$  nonuniformity (heterogeneity), if present, means that the FA distribution is also nonuniform. There are two primary causes of such nonuniformity. Firstly, dielectric resonance produces standing waves in the subject, which are more pronounced at higher fields ( $\geq 3T$ ), and in larger objects (the effect is greater in the body than in the head). Secondly, smaller transmit coils are less uniform, and therefore the body transmit coil is to be preferred (not a smaller combined transmit/receive coil). During the FA setup procedure, a good technique will optimise the FA over just the volume to be imaged (not the whole slice), and an accurate FA may then be obtained in spite of more global FA nonuniformity. An additional source of FA error is in 2D multislice imaging, where the slice profile is often poor, and a

distribution of FA values exists across the slice. Therefore 3D (volume) acquisitions are preferred.  $B_1$  maps can be measured quite quickly [12] (<2 min) and these may enable corrections to be made in the presence of FA inaccuracy and inhomogeneity. Phased transmit array technology is in development (essential for imaging  $>3T$ ). This gives impressive control over  $B_1$  at each location in the subject, and such ‘RF shimming’ is expected to give uniform and accurate FA values. The tissue  $T_1$  value ( $T_{10}$ ) can be measured, or else a standard value from the literature used. An accurate measurement is preferred for each individual subject, since in disease this can alter; this can often be carried out in < 5 minutes. The most common method is the variable flip angle method, where gradient echo sequences with several FA values are used. These include a mostly PD-weighted sequence (low FA) and one or more  $T_1$ -weighted sequence (higher FA). Clearly the  $T_{10}$  accuracy is crucially dependent on the FA accuracy. Inversion recovery methods (with variable TI, fixed FA) are more robust, but usually slower. The measured  $K^{trans}$  value is very sensitive to the accuracy of the  $T_{10}$  value. An example from breast cancer shows that [13] for a range of feasible  $T_{10}$  values, the fits are equally good,  $K^{trans}$  can vary by at least a factor of 2, and  $v_e$  can reach impossible values ( $v_e > 100\%$ ); see table 1.  $k_{ep}$  is relatively robust. An increase of 1% in  $T_{10}$  gives a resulting decrease of 1% in  $K^{trans}$ , such that the product remains approximately constant. Any low molecular weight contrast agent can in principle be used for DCE methodology. The initial work [5] was carried out with Gd-DTPA, size 570D, and then with Magnevist (938D). Clearly larger molecules will have lower permeability and hence  $K^{trans}$  values, and the AIF may alter a little with viscosity. In view of the con-

cerns about NSF, there will be value in gaining experience using the newer cyclic compounds. Potentially suitable candidate compounds are as follows. Dotarem (754D), Eovist (725D), Gadovist (605D), Magnevist (938D), Multihance (1058D), Omniscan (574D), Opti-mark (662D), Primovist (685D), Prohance (559D) and Teslascan (757D) (see <http://www.rxlist.com>).

5. Image analysis

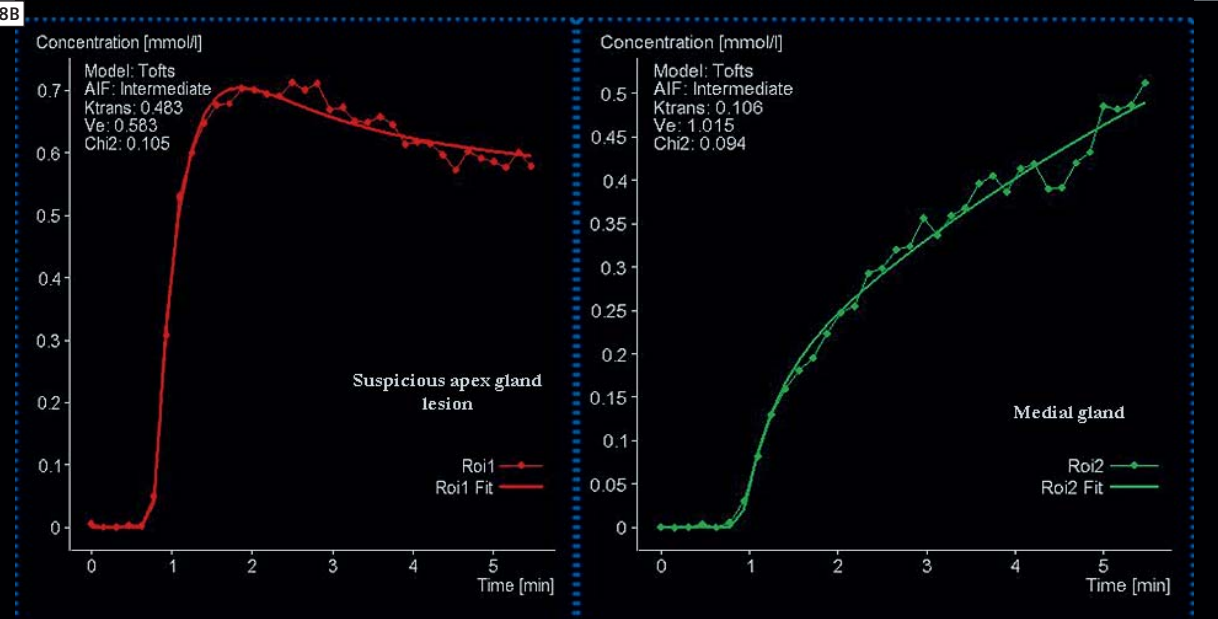
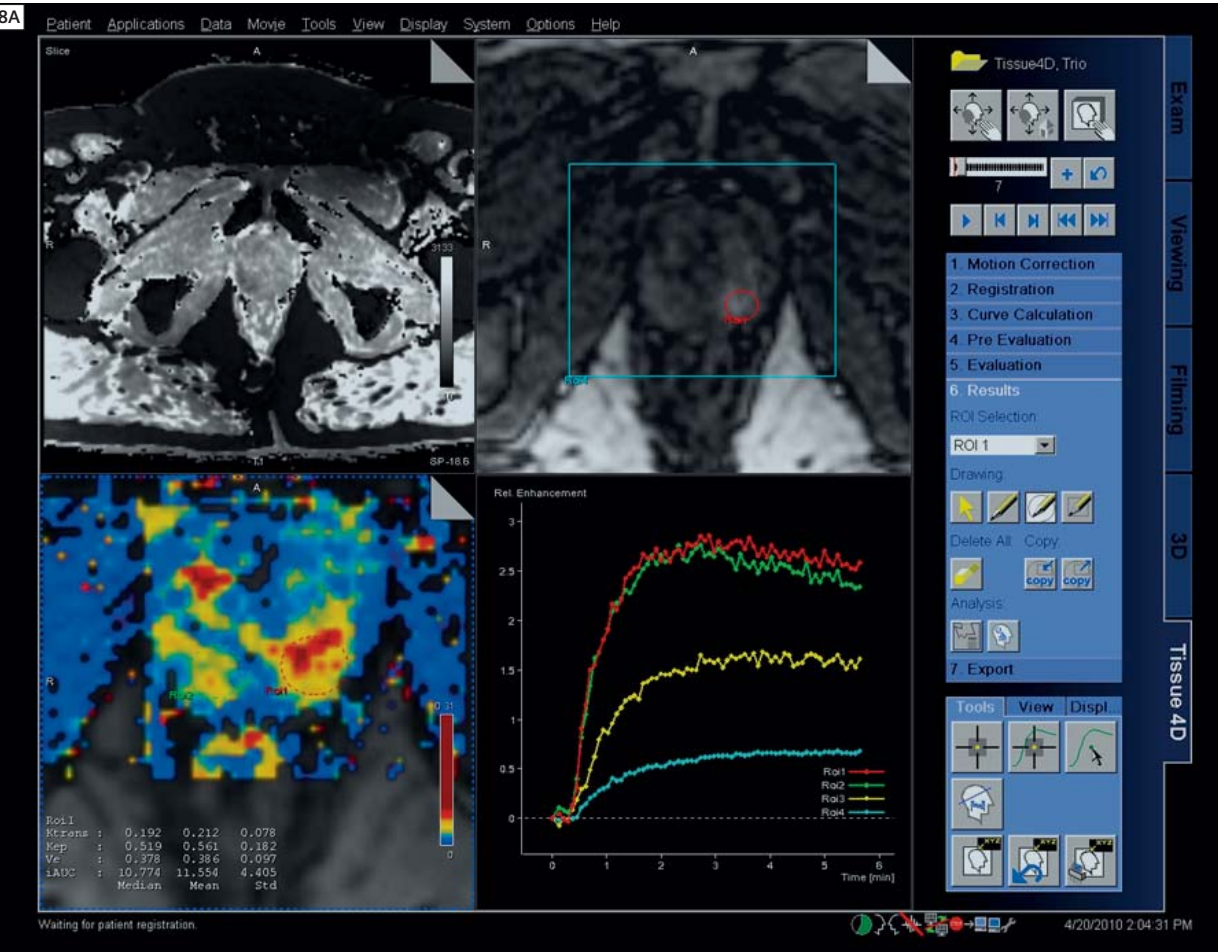
Analysis can be carried out on individual ROI’s, or on a pixel-by-pixel basis to produce a map for the whole organ. The reduction of motion artefact using spatial registration, if available, is likely to improve the quality of the fit (depending on the tissue location). Because the motion is non-rigid, effective removal is much harder than in the brain, and a topic of ongoing research. In-plane movement is relatively easy to reduce. The pharmacokinetic model requires knowledge of the arterial plasma concentration  $C_p(t)$ ; this arterial input function (AIF) can be calculated from the blood signal (which confusingly can also be called the AIF!). It can be measured for each subject, and thus within- and between-subject variation can be taken into account, although if the technique is not implemented well it can introduce extra variation which contaminates the final measurements of tissue physiology. Alternatively a population average AIF can be used. Some of these are described analytically (i.e. using mathematical equations, rather than just a list of numbers), which makes them more convenient to use. In particular they are available at any temporal resolution. The most popular are the original biexponential Weinmann plasma curve [5], derived from low temporal resolution arterial blood samples, and the more complex Parker blood function [11], derived from high temporal resolution MRI data. In the Parker function, bolus first pass and recirculation are represented. After bolus passage and recirculation, the MRI measurement (Parker  $C_p(1 \text{ min}) = 1.53 \text{ mM}$  assuming Hct = 42%) is 86% higher than the direct measurement (Weinmann  $C_p(1 \text{ min}) = 0.82 \text{ mM}$ ). The possible reasons for this discrepancy include a population difference and wash-in effects in the MRI method. The numerical AIF’s of Fritz-Hansen [14] showed excellent agreement between an inversion recovery MRI method and direct blood measurements; their values (average over 6 subjects  $C_p(1 \text{ min}) = 1.09 \text{ mM}$ ) are closer to the Weinmann value. The choice of AIF will depend on the tissue being studied and the sequences available. When it comes to the modelling, several versions can be considered. The primary free parameters are  $K^{trans}$  and either  $k_{ep}$  or  $v_e$  (since  $k_{ep}$  and  $v_e$  are related). It is



worth including  $v_p$  to see if the fit improves. The onset time of the bolus  $t_{onset}$  will be needed if a population average AIF is used (since the timing of bolus arrival with respect to the start of tissue enhancement is unknown). The appropriate approach will again depend on the organ and the temporal resolution. The mathematical process of fitting the model to the data works as follows. The model signal can be calculated for many combinations of the free parameters ( $K^{trans}$  etc. see table 2 below). For each of these combinations, the differences between the model signal value (at each time point) and the measured data are found. These differences are squared and summed across each time point to provide a ‘total difference’. The free parameters are adjusted until this total difference is minimised. The model has then been ‘fitted’ to the data. This is called the ‘least squares solution’. The differences between the data and the fitted model are called ‘residuals’ (see e.g. fig. 5). From these can be found the ‘root-mean-square residual’, which is a kind of average difference between the model and the data, and which gives an indication of the quality of the model and of the fit. If the residuals appear random in character then these probably derive from a random effect such as image noise or movement; if there seems to be a systematic pattern to the residuals then the model can often be improved. ‘Fit failures’ can occur, particularly if the data are noisy (e.g. deriving from single pixels instead of a ROI); no

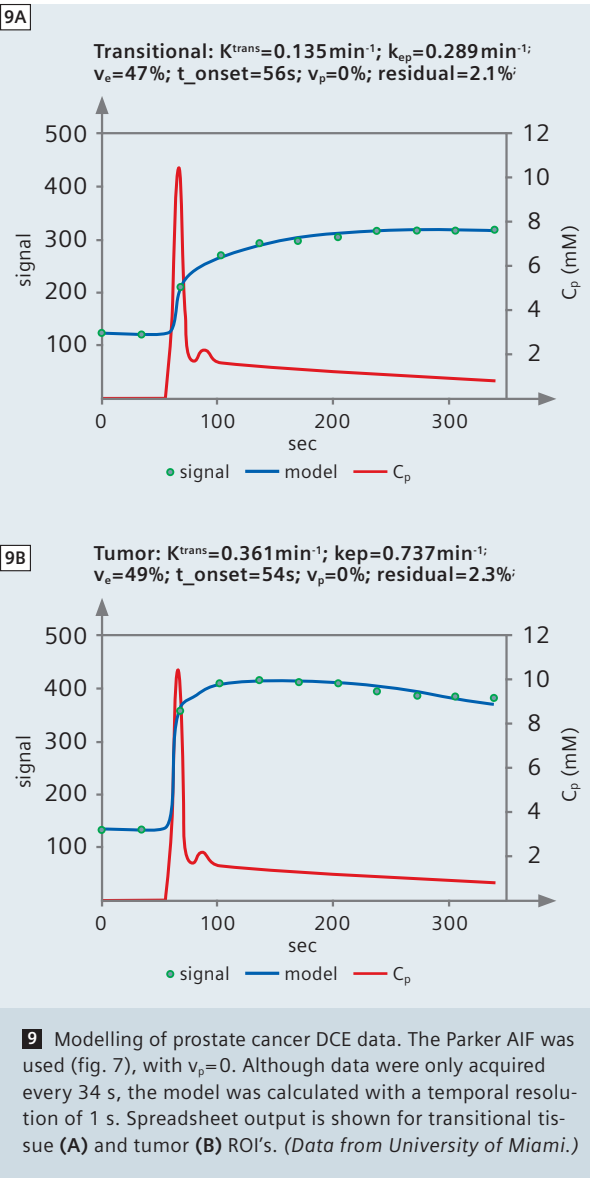
Table 1: Sensitivity of tissue parameters to $T_{10}$ value. (Adapted from Tofts 1995 [13])						
Tissue	$T_{10}$ (s)	$K^{trans}$ (min <sup>-1</sup> )	$v_e$ (%)	residual in fit	$k_{ep}$ (min <sup>-1</sup> )	$K^{trans} T_{10}$
Normal low risk fatty portion	0.46	0.88	143	0.091	0.62	0.41
Tumor – low $T_1$	0.60	0.63	96	0.092	0.65	0.38
Normal high risk diffuse density portion	0.71	0.51	76	0.093	0.67	0.36
Tumor – high $T_1$	1.3	0.26	36	0.095	0.72	0.34





8 (A) Tissue4D output. The workflow includes motion correction and registration. (B) Fit to data from prostate ROI's.

valid parameter values are produced for that dataset. In the fitting process it is important to identify and flag these failures, so that the output (i.e. invalid parameter values) does not contaminate any subsequent analysis. Values of  $v_e > 100\%$  may occur if an incorrect value of  $T_{10}$  has been used (see table 1), or if the enhancement peak has not been reached (see fig. 3B). Fitting can be implemented in two ways. The simplest way is to use ROI data (which are inherently low noise) and put these into a spreadsheet (e.g. Microsoft Excel running on a PC). The mathematics can be set up using inbuilt formula functions, and the 'solver' function can carry out the minimisation process. This does of course require some mathematical and computer ability. The more complex way is to set up pixel-by-pixel mapping, either using a standard environment (e.g. matlab) or by obtaining this from a supplier. Pixel mapping almost certainly needs spatial registration of the images to reduce the effect of motion; the operation is much more computer-intensive, and the single-pixel data are inherently noisy, so care must be taken to identify fit failures. The benefits of pixel mapping include the abilities to interrogate all the tissue without bias, and to generate histograms. Histograms can show the distribution of parameter values, in a Region- or Volume-of-Interest. By taking care of histogram generation and architecture, histograms become more useful and comparisons are more easily made [15]. The y-values can be calculated such that the area under the histogram curve is either the total volume under interrogation (in mL), or 100%. By taking account of bin width, the histogram amplitude becomes virtually independent of bin width, and in a multicenter brain MTR study the intercenter difference was completely eliminated [16]. Features such as peak location and height can be extracted from histograms. Characterising the distribution tails can have predictive value [17, 18], and principle component analysis of the histogram shape can be powerful [19]. An example of a quite comprehensive software package to carry out pixel-by-pixel analysis is Tissue4D (fig. 8). The various functions needed are provided in a single workflow scheme, and ROI analysis is also available (this is useful to evaluate the quality of the modelling). An example of using a spreadsheet to implement modelling of ROI data is shown in figure 9. The prostate data have quite low temporal resolution (34 s),  $T_{10}$  had to be assumed (1.5 s), and a Parker AIF was used. Including the  $v_p$  term did not improve the fitting (and in fact it became rather unstable). In several ROI's from the same subject, fitted onset time agreed within 2 s, suggesting that it can be found quite reliably.



## 6. Conclusions

The principle physiological parameters that can be measured with DCE-MRI are the transfer coefficient  $K_{trans}$  (related to capillary permeability, surface area and perfusion) and  $v_e$  the size extravascular extracellular space. To do this needs good control of flip angle and an accurate measurement of tissue  $T_1$  before injection of Gd. If  $T_1$  is not available, then it may be possible to use a standard value; in any case the rate constant  $k_{ep}$  can still be measured, which is probably useful. The possible and optimum acquisition protocols and models will depend on which tissue is being imaged. Spreadsheet analysis can provide quick access to modelling.

Acknowledgements

David Collins, Martin Leach and David Buckley contributed valuable insight into DCE imaging. Isky Gordon (University College London) and Iosif Mendichovszky provided data for figure 5. Peter Gall (Siemens Healthcare) contributed figure 8 and the list of CA’s. Radka Stoyanova (University of Miami) provided data for figure 9.

Appendix

MRI model  
T<sub>1</sub> is reduced from its native value T<sub>10</sub> by the presence of a concentration C of Gd:

$$\frac{1}{T_1} = \frac{1}{T_{10}} + r_1 C$$

Equation 1

r<sub>1</sub> is the relaxivity, and usually an in-vitro value of 4.5 s<sup>-1</sup> mM<sup>-1</sup> is used. Often it is more convenient to use the relaxation rate:

$$R_1 = R_{10} + r_1 C$$

Equation 2

Note that to apply eqns 1 and 2 to total tissue Gd concentration implicitly assumes fast exchange i.e. that all the Gd in a voxel is available to relax all of the water. The signal S from a spoilt gradient echo sequence (i.e. FLASH) is:

$$S = S_0 \frac{(1 - e^{-TR/T_1}) \sin \theta}{1 - e^{-TR/T_1} \cos \theta}$$

Equation 3

where S<sub>0</sub> is the relaxed signal (TR>>T<sub>1</sub>, θ=90°), and θ is the FA. S<sub>0</sub> can be found from the measured pre-Gd signal (before injection of CA).

References

1 Jackson A, Buckley DL, Parker GJ. Dynamic Contrast-Enhanced Magnetic Resonance Imaging in Oncology. Springer, 2004.  
2 Tofts PS. Quantitative MRI of the brain: measuring changes caused by disease. John Wiley, 2003.  
3 Tofts PS, Brix G, Buckley DL, Evelhoch JL, Henderson E, Knopp MV, Larsson HB, Lee TY, Mayr NA, Parker GJ, Port RE, Taylor J, Weisskoff RM. Estimating kinetic parameters from dynamic contrast-enhanced T(1)-weighted MRI of a diffusable tracer: standardized quantities and symbols. J Magn Reson Imaging 1999;10:223-232.

To find the plasma concentration (if required), firstly the blood concentration C<sub>b</sub>(t) is found from the blood signal, using eqns 1 and 3. Blood T<sub>10</sub> is about 1.4 s [20]. The plasma concentration C<sub>p</sub>(t) is higher, by a factor related to the haematocrit Hct (typically 42%):

$$C_p = \frac{C_b}{1 - Hct}$$

Equation 4

Pharmacokinetic model

The flow of Gd across the endothelium into the EES is

$$v_e \frac{dC_e(t)}{dt} = K^{trans} (C_p(t) - C_e(t))$$

Equation 5

The solution to this is [7] a convolution of C<sub>p</sub> with the impulse response function K<sup>trans</sup> exp(-k<sub>ep</sub>t); when the IV Gd is taken into account, the total tissue concentration is:

$$C_t(t) = v_p C_p(t) + K^{trans} \int_0^t C_p(\tau) e^{-k_{ep}(t-\tau)} d\tau$$

Equation 6

Model parameters

There are several kinds of parameters used in the model. *Fixed* parameters (FA TR Hct T<sub>10</sub> T<sub>10</sub><sup>blood</sup> r<sub>1</sub>) have preset values which are required before fitting can start. *Free* parameters (K<sup>trans</sup> v<sub>e</sub> k<sub>ep</sub> and maybe v<sub>p</sub> and t<sub>onset</sub>) are varied and then estimated as part of the fitting process. Other parameters (C<sub>p</sub> etc) are used temporarily as part of the process of modelling the signal. The fixed and free parameters are summarised in table 2.

4 Leach MO, Brindle KM, Evelhoch JL, Griffiths JR, Horsman MR, Jackson A, Jayson GC, Judson IR, Knopp MV, Maxwell RJ, McIntyre D, Padhani AR, Price P, Rathbone R, Rustin GJ, Tofts PS, Tozer GM, Vennart W, Waterton JC, Williams SR, Workman P. The assessment of antiangiogenic and antivascular therapies in early-stage clinical trials using magnetic resonance imaging: issues and recommendations. Br J Cancer 2005;92:1599-1610.  
5 Tofts PS, Kermode AG. Measurement of the blood-brain barrier permeability and leakage space using dynamic MR imaging. 1. Fundamental concepts. Magn Reson Med 1991;17:357-367.

Table 2: Fixed and free parameters in DCE modelling.

Quantity	symbol	units	type
flip angle <sup>a</sup>	FA	degrees	fixed
haematocrit	Hct	%	fixed (42%)
onset time	t <sub>onset</sub>	s	free
rate constant <sup>b</sup>	k <sub>ep</sub>	min <sup>-1</sup>	free
transfer constant	K <sup>trans</sup>	min <sup>-1</sup>	free
T <sub>1</sub> relaxivity	r <sub>1</sub>	s <sup>-1</sup> mM <sup>-1</sup>	fixed (4.5 s <sup>-1</sup> mM <sup>-1</sup> )
T <sub>1</sub> of blood	T <sub>10</sub> <sup>blood</sup>	s	fixed (1.4 s)
T <sub>1</sub> of tissue	T <sub>10</sub>	s	fixed
TR	TR	s	fixed
fractional volume of EES <sup>c</sup>	v <sub>e</sub>	0<v <sub>e</sub> <100%	free
fractional volume of blood plasma in tissue	v <sub>p</sub>	0<v <sub>p</sub> <100%	free

<sup>a</sup>θ is the flip angle in radians, <sup>b</sup>k<sub>ep</sub> = K<sup>trans</sup>/v<sub>e</sub>, <sup>c</sup>Extravascular Extracellular Space

6 Kety SS. The theory and applications of the exchange of inert gas at the lungs and tissues. Pharmacol Rev 1951;3:1-41.  
7 Tofts PS. Modeling tracer kinetics in dynamic Gd-DTPA MR imaging. J Magn Reson Imaging 1997;7:91-101.  
8 St Lawrence KS, Lee TY. An adiabatic approximation to the tissue homogeneity model for water exchange in the brain: I. Theoretical derivation. J Cereb Blood Flow Metab 1998;18:1365-1377.  
9 Donaldson SB, West CM, Davidson SE, Carrington BM, Hutchison G, Jones AP, Sourbron SP, Buckley DL. A comparison of tracer kinetic models for T1-weighted dynamic contrast-enhanced MRI: application in carcinoma of the cervix. Magn Reson Med 2010;63:691-700.  
10 Tofts PS, Cutajar M, Mendichovszky IA, Gordon I. Accurate and precise measurement of renal filtration and vascular parameters using DCE-MRI and a 3-compartment model. Proc Intl Soc Mag Reson Med, 18th annual meeting, Stockholm.2010; 326.  
11 Parker GJ, Roberts C, Macdonald A, Buonaccorsi GA, Cheung S, Buckley DL, Jackson A, Watson Y, Davies K, Jayson GC. Experimentally-derived functional form for a population-averaged high-temporal-resolution arterial input function for dynamic contrast-enhanced MRI. Magn Reson Med 2006;56:993-1000.  
12 Dowell NG, Tofts PS. Fast, accurate, and precise mapping of the RF field in vivo using the 180 degrees signal null. Magn Reson Med 2007;58:622-630.  
13 Tofts PS, Berkowitz B, Schnall MD. Quantitative analysis of dynamic Gd-DTPA enhancement in breast tumors using a permeability model. Magn Reson Med 1995;33:564-568.  
14 Fritz-Hansen T, Rostrup E, Larsson HB, Sondergaard L, Ring P, Henriksen O. Measurement of the arterial concentration of Gd-DTPA using MRI: a step toward quantitative perfusion imaging. Magn Reson Med 1996;36:225-231.  
15 Tofts PS, Davies GR, Dehmshki J. Histograms: measuring subtle diffuse disease (chapter 18). In: Paul Tofts, editor. Quantitative MRI of the brain: measuring changes caused by disease. Chichester: John Wiley, 2003: 581-610.  
16 Tofts PS, Steens SC, Cercignani M, Admiraal-Behloul F, Hofman PA, van Osch MJ, Teeuwisse WM, Tozer DJ, van Waesberghe JH, Yeung R, Barker GJ, van Buchem MA. Sources of variation in multi-centre brain MTR histogram studies: body-coil transmission eliminates inter-centre differences. Magn Reson Mater Phy 2006;19:209-222.  
17 Tofts PS, Benton CE, Weil RS, Tozer DJ, Altmann DR, Jager HR, Waldman AD, Rees JH. Quantitative analysis of whole-tumor Gd enhancement histograms predicts malignant transformation in low-grade gliomas. J Magn Reson Imaging 2007;25:208-214.  
18 Donaldson SB, Buckley DL, O'Connor JP, Davidson SE, Carrington BM, Jones AP, West CM. Enhancing fraction measured using dynamic contrast-enhanced MRI predicts disease-free survival in patients with carcinoma of the cervix. Br J Cancer 2010;102:23-26.  
19 Dehmshki J, Ruto AC, Arridge S, Silver NC, Miller DH, Tofts PS. Analysis of MTR histograms in multiple sclerosis using principal components and multiple discriminant analysis. Magn Reson Med 2001;46:600-609.  
20 Spees WM, Yablonskiy DA, Oswood MC, Ackerman JJ. Water proton MR properties of human blood at 1.5 Tesla: magnetic susceptibility, T(1), T(2), T\*(2), and non-Lorentzian signal behavior. Magn Reson Med 2001;45:533-542.

Contact

Professor Paul Tofts  
Clinical Imaging Sciences Centre  
Brighton and Sussex Medical School  
University of Sussex  
Brighton  
BN1 9PX  
United Kingdom  
Website: www.paul-tofts-phd.org.uk  
dce@paul-tofts.org.uk



## Global Siemens Headquarters

Siemens AG  
Wittelsbacherplatz 2  
80333 Muenchen  
Germany

[www.siemens.com/healthcare-magazine](http://www.siemens.com/healthcare-magazine)

Order No. A91MR-1000-78C-7600 | Printed in Germany | CC MR 01000 ZS 111020. | © 11.10, Siemens AG

On account of certain regional limitations of sales rights and service availability, we cannot guarantee that all products included in this brochure are available through the Siemens sales organization worldwide. Availability and packaging may vary by country and is subject to change without prior notice. Some/All of the features and products described herein may not be available in the United States.

The information in this document contains general technical descriptions of specifications and options as well as standard and optional features which do not always have to be present in individual cases.

Siemens reserves the right to modify the design, packaging, specifications and options described herein without prior notice.  
Please contact your local Siemens sales representative for the most current information.

Note: Any technical data contained in this document may vary within defined tolerances. Original images always lose a certain amount of detail when reproduced.

## Global Business Unit

Siemens AG  
Medical Solutions  
Magnetic Resonance  
Henkestr. 127  
DE-91052 Erlangen  
Germany  
Phone: +49 9131 84-0  
[www.siemens.com/healthcare](http://www.siemens.com/healthcare)

## Local Contact Information

### In Asia

Siemens Pte Ltd  
The Siemens Center  
60 MacPherson Road  
Singapore 348615  
Phone: +65 6490-8096

### In Canada

Siemens Canada Limited  
Medical Solutions  
2185 Derry Road West  
Mississauga ON L5N 7A6  
Canada  
Phone: +1 905 819-5800

### Europe/Africa/Middle East

Siemens AG  
Medical Solutions  
Henkestr. 127  
91052 Erlangen  
Germany  
Phone: +49 9131 84-0

### Latin America

Siemens S.A.  
Medical Solutions  
Avenida de Pte. Julio A. Roca No 516,  
Piso 7  
C1067ABN Buenos Aires  
Argentina  
Phone: +54 11 4340-8400

### USA:

Siemens Medical Solutions U.S.A., Inc.  
51 Valley Stream Parkway  
Malvern, PA 19355-1406  
USA  
Phone: +1-888-826-9702